DEUTSCHES ELEKTRONEN-SYNCHROTRON DESY

DESY 81-013
March 1981

EXPERIMENTAL EVIDENCE ON QCD

by

P. Söding and G. Wolf

NOTKESTRASSE 85 · 2 HAMBURG 52

To be sure that your preprints are promptly included in the
HIGH ENERGY PHYSICS INDEX ,
send them to the following address (if possible by air mail) :

DESY
Bibliothek
Notkestrasse 85
2 Hamburg 52
Germany

DESY 81-013
March 1981

EXPERIMENTAL EVIDENCE ON QCD

P.Söding and G.Wolf

Deutsches Elektronen-Synchrotron DESY, Hamburg

Contents

To be published in

Annual Review of Nuclear and Particle Science

1. INTRODUCTION

In our present understanding hadronic matter consists of quarks bound together by colour fields in much the same way proton and electron are bound by the electromagnetic field in the hydrogen atom. Quarks, in addition to their electric and weak charges, carry colour charge which takes three values (Greenberg 1964, Han & Nambu 1965). Hadrons are assumed to be colour singlets (Bardeen et al. 1973). Gluons, the quanta of the colour field, are colour octet states coupled to the colour triplet charges of quarks. The interaction between quarks and gluons is described by Quantum Chromodynamics (QCD) (Nambu 1966, Fritzsch & Gell-Mann 1972, Fritzsch et al. 1973, Weinberg 1973, Gross & Wilczek 1973; for a review see Marciano & Pagels 1978).

The evidence for the quark composition of hadrons is based on the spectroscopy of hadrons, on the structure of nucleons as revealed in inelastic lepton scattering, and on results from e^+e^- annihilation into hadrons. The spectroscopy data imply that mesons are $q\bar{q}$ systems - shown beautifully in the charmonium system - and baryons consist of three quarks. Initial problems with the statistics of baryons (notably the Δ^{++}) got resolved when the colour degree of freedom was introduced. Direct evidence for pointlike charged constituents of the nucleon is provided by the observation (see e.g. Taylor 1969) of approximate scaling (Bjorken 1969) in lepton nucleon scattering. The angular dependence of the scattering shows the spin of the constituents to be 1/2, and comparison between electron and neutrino scattering allows to determine the average squared charge of the constituents. Putting everything together one finds that the constituents, or partons, fit the warrant for quarks (Feynman 1972). In addition, lepton nucleon scattering provides evidence for neutral partons in the nucleon which are thought to be gluons.

If quarks are permanently confined in hadrons and unobservable as free particles (see, however, LaRue et al. 1979), then the nearest approach to observing a free isolated quark is to observe the jet of hadrons into which a quark fragments. The clearest evidence for jets is found in e^+e^- annihilation at high energies (Hanson et al. 1975). These jets emerge back-to-back with an angular distribution identical to that for

the production of pointlike spin 1/2 particles (Schwitters et al. 1975), and the total jet production cross section is equal to the cross section expected for production of pointlike coloured quark-antiquark pairs. Long range charge correlations between opposite jets confirm that the jets arise from charged parent particles (Brandelik et al. 1981a). The obvious interpretation of these results is that e^+e^- annihilation first produces $q\bar{q}$ pairs which subsequently fragment into hadrons, producing the two distinct jets.

The gluons predicted by QCD are more difficult to observe. They are massless, flavourless, neutral vector partons. Since QCD is a nonabelian gauge theory, the gluons are coloured and interact with each other. The quark gluon coupling is described by an effective coupling constant g_{eff} that depends on the characteristic momentum transfer Q of the process; in leading order of perturbation theory it is given by

$$\alpha_s(Q^2) \equiv \frac{g_{eff}^2}{4\pi} = \frac{12\pi}{(33 - 2N_f)\,\ell n Q^2/\Lambda^2} \qquad (1.1)$$

Here N_f is the number of active quark flavours (e.g. $N_f = 5$ for u,d,s, c,b) and Λ is the QCD scale parameter. The coupling strength decreases with increasing Q^2, consistent with asymptotic freedom at large Q^2. For low Q^2 or large distances the coupling strength increases until perturbation theory becomes invalid; eventually confinement may arise.

It is the short distance region where perturbative methods apply and QCD can be directly confronted with experiment (for a recent review see Llewellyn Smith 1980). Particularly fruitful areas, in this respect, have been deep-inelastic lepton nucleon scattering, quarkonium decay, and jet production in e^+e^- annihilation. In these processes effects are seen that are naturally interpreted as the traces of gluons radiated by strongly accelerated quarks. This evidence will be the subject of our presentation, which should be considered a status report on a rapidly developing field. We restrict ourselves to the above mentioned processes; other applications of QCD such as large P_T processes and lepton pair production by hadron hadron scattering are beyond the scope of this review.

2. DEEP-INELASTIC LEPTON NUCLEON SCATTERING

About a decade ago experiments on electron nucleon scattering have revealed the approximate scale invariance of the nucleon structure functions (for a review see Friedman & Kendall 1972). This scaling behaviour (Bjorken 1969) provided convincing evidence for the existence of virtually free, pointlike constituents of the nucleon (Feynman 1972). The success of the quark-parton model in describing these results was later interpreted as being a consequence of asymptotic freedom, suggesting a nonabelian gauge field theory of the strong interactions ('t Hooft 1972, Politzer 1973, Gross & Wilczek 1973). In field theories of the strong interactions, however, scaling is not expected to hold exactly because of gluonic radiative corrections. In recent scattering experiments the range of momentum transfers has been extended to $Q^2 \sim 200\ \mathrm{GeV}^2$ and evidence for these corrections has been found. The quantitative interpretation can provide stringent tests of QCD. We will in this section concentrate on scale breaking in nucleon structure functions. Effects of gluon radiation are also expected to show up in the final state hadron distributions; these are the subject of the paper by Renton & Williams (1981).

The diagrams describing deep-inelastic scattering in lowest weak or electromagnetic order are shown in Fig. 2.1. We will discuss charged current ν and $\bar{\nu}$ and electromagnetic e and μ scattering experiments. Interference with the weak neutral current, as well as two photon exchange, can be neglected. The final state partons (quarks, gluons) and the "spectator" remnants from the incident nucleon are assumed to develop into jets of hadrons. Only the initial ℓN state and the final lepton ℓ' is kinematically fixed; apart from the total c.m. energy ($s = (p_\ell + P_N)^2$) there are then two kinematical variables

$$q^2 = (p_\ell - p_{\ell'})^2 = -Q^2 = \text{square of four-momentum transfer}$$
$$W^2 = (q + p_N)^2 = \text{total mass of final hadronic system squared}$$

or equivalently

$$x = \frac{Q^2}{2(q\cdot p_N)} = \frac{Q^2}{2m_N\nu}$$ the Bjorken scaling variable (in the laboratory system, ν = energy transfer)

$$y = \frac{(q\cdot p_N)}{(p_\ell\cdot p_N)} = \frac{\nu}{E_\ell}$$ the fraction of the laboratory energy E_ℓ of the incident lepton transferred to the exchanged current.

At high energy ($s >> m_N^2$) neglecting lepton masses, $Q^2 \approx xys$, $W^2 \approx Q^2(1/x-1) + m_N^2$, and the differential cross section for neutrino and antineutrino scattering is given by

$$\frac{d^2(\sigma^\nu + \sigma^{\bar\nu})}{dxdy} = \frac{G^2 s}{2\pi} F_2(x,Q^2)\left[1 + (1-y)^2 - \frac{y^2}{1 + 1/\tilde R(x,Q^2)}\right]$$

$$\frac{d^2(\sigma^\nu - \sigma^{\bar\nu})}{dxdy} = \frac{G^2 s}{2\pi} xF_3(x,Q^2)\left[1 - (1-y)^2\right] \qquad (2.1)$$

while for charged lepton scattering

$$\frac{d^2\sigma^{e,\mu}}{dxdy} = \frac{2\pi\alpha^2 s}{Q^4} F_2(x,Q^2)\left[1 + (1-y)^2 - \frac{y^2}{1 + 1/\tilde R(x,Q^2)}\right] \qquad (2.2)$$

where $F_i(x,Q^2)$ are the nucleon structure functions for interaction with the charged weak (in eq. (2.1)) or the electromagnetic current (in eq.(2.2)) respectively, and

$$\tilde R(x,Q^2) = F_2(x,Q^2)/2xF_1(x,Q^2) - 1 \qquad (2.3)$$

is approximately[1] equal to $R \equiv \sigma_L/\sigma_T$. In the limit of quasi-free quark partons, $\tilde R \equiv 0$. Equation (2.1) is written for an isoscalar target, assuming charge symmetry of the structure functions. (This is not exactly valid, since there is a small correction from the difference between the strange and charmed quark sea.) The electromagnetic and weak structure functions are closely related (see eqn.(2.4)).

In the ideal case of equal incident ν and $\bar\nu$ fluxes, the experimental determination of xF_3 according to eqn.(2.1) is straightforward. On

1) The precise relation is $R \equiv \sigma_L/\sigma_T = (1 + 4x^2m_N^2/Q^2)F_2/2xF_1 - 1$.

the other hand, the determination of F_2 depends on the value of $R(x,Q^2)$. Obviously, R can be obtained from an analysis of the y dependence of the cross sections at fixed x and Q^2, by varying the total energy $\sqrt{s}$. Its precise dependence on x and Q^2 is not yet known; average measured values are $R = 0.10 \pm 0.025$ (statistic) ± 0.07 (systematic) for neutrino scattering ($0 < x < 0.6$, $2 < Q^2 < 200$ GeV^2), or $R = 0.21 \pm 0.10$ for electron scattering ($0.1 < x < 0.9$, $2 < Q^2 < 20$ GeV^2) (de Groot et al 1980, Mestayer 1978).

In the quark-parton picture of Fig. 2.1a, the scattering is described at high s as incoherent elastic scattering on the quasi-free pointlike quark constituents of the nucleon. In this description, x is the fractional momentum carried by the struck quark. The structure functions will scale, i.e. depend only on x. In terms of the quark distribution functions u(x), d(x),... for the different flavours in the nucleon, they are given by

$$\begin{aligned} F_2(x) = 2xF_1(x) &= x[q(x) + \bar{q}(x)], \\ xF_3(x) &= x[q(x) - \bar{q}(x)] \end{aligned} \qquad (2.4)$$

where for the weak current $q(x) = u(x) + d(x) + s(x) + c(x)$. In the electromagnetic structure functions each flavour is weighted by the square of the quark charge, $q(x) = \frac{4}{9}u(x) + \frac{1}{9}d(x) + \frac{1}{9}s(x) + \frac{4}{9}c(x)$. To $F_3(x)$ only the valence quarks but not the $q\bar{q}$ sea contribute, and it is therefore a flavour nonsinglet. By contrast, $F_2(x)$ measures all quarks and antiquarks in the nucleon, i.e. it contains a flavour-singlet component.

It has long been known that exact scaling as predicted by the quark-parton model does not hold (Fox et al. 1974, Riordan et al. 1974, Atwood et al. 1976, Anderson et al. 1977). This is in fact expected, since in field theories of the strong interaction real and virtual field quanta can be emitted as shown in leading order in Fig. 2.1(b)-(e). The diagram of Fig. 2.1(e) changes only the final hadronic distribution over which we integrate; the other diagrams will lead to scale-breaking. The qualitative pattern of the scaling violation can intuitively be understood (Kogut & Susskind 1974). As Q^2 is raised, the resolving power

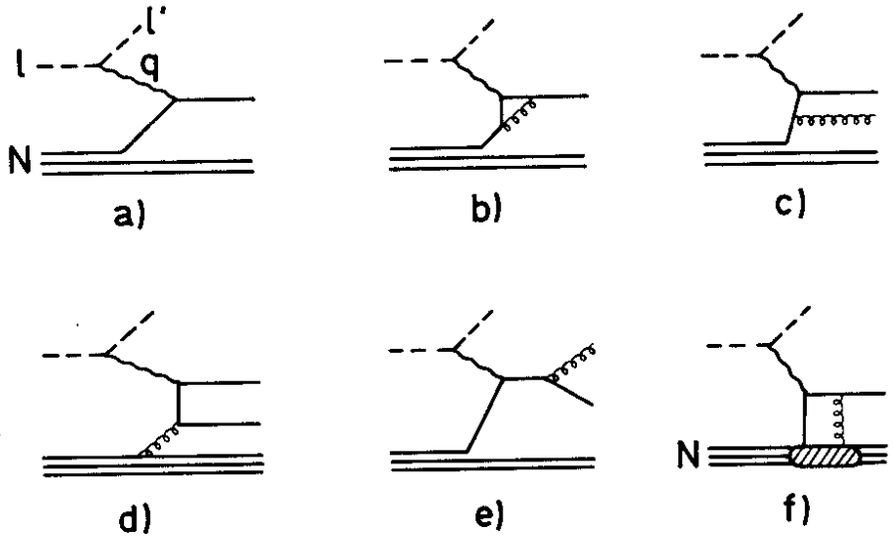

25 02 81 32284

Fig. 2.1 Deep-inelastic lepton-nucleon scattering is described by (a) the simple quark-parton model, (b) - (e) leading order gluonic radiative corrections to (a), and (f) higher order twist contributions.

of the probing current increases and quarks begin to appear as systems composed of quarks plus clouds of gluons or $q\bar{q}$ pairs. The fractional momentum x carried by the quark that is probed will thus appear smaller. Consequently the quark distribution function q(x) will shrink towards smaller values of x.

The ensuing QCD corrections to the basic quark parton scaling property can be calculated by perturbative methods (Gross & Wilczek 1973, Georgi & Politzer 1974). The structure functions are predicted to fall logarithmically with Q^2 for large x and to rise for small x. The only unknown parameter involved in the prediction is the QCD scale parameter Λ that describes the Q^2-dependent quark gluon coupling $\alpha_s(Q^2)$.

Apart from these gluonic radiative corrections, other types of scale breaking contributions to the structure functions are expected which vary like powers of $1/Q^2$. Such contributions arise from the bound state nature of the nucleon target, involving interactions of the struck quark with other partons of the target as in Fig. 2.1(f). These higher order twist contributions cannot be calculated perturbatively. Estimation of their size is only possible in the framework of specific models. For quantitative checks of QCD these contributions must therefore be isolated from the perturbative effects. In principle the different Q^2 dependence of the scaling violations - power of $1/Q^2$ vs. $\ell n Q^2$ - should allow a separation between the higher twist contributions and the gluonic radiative corrections to the leading twist term. The higher twist effects are expected to be particularly important at large x. The observed scaling violations in the Q^2 region up to ~20 GeV^2 may in fact be largely dominated by these effects although this is not unanimously agreed upon (Abbott & Barnett 1980, Donnachie & Landshoff 1980, Duke & Roberts 1980, Glück & Reya 1980, Pennington & Ross 1981, Jaffe & Ross 1980). The data have also been fitted using a different form of subasymptotic corrections motivated by the massive quark model (Castorina et al. 1980).

Another source of scaling violations is the onset of the production of heavy quarks above some threshold in W. At fixed x, this will cause structure functions to rise with increasing Q^2. The production of charm in deep-inelastic muon scattering has been investigated by the Berkeley-

Fermilab-Princeton collaboration (Clark et al. 1980) and by the European Muon Collaboration (Aubert et al. 1980). These groups conclude that $c,\bar{c}$ production is responsible for a significant part of the scaling violations seen in $F_2(x,Q^2)$ at low values of x (see also Donnachie & Shaw 1980).

For these reasons, the comparison of the scale breaking effects in the nucleon structure functions with the predictions of perturbative QCD has to rely on data from the region of high Q^2 and neither too small nor too large values of x. This is unfortunately the region of x where the logarithmic QCD effects are smallest. The QCD predictions and the problems of comparing them with data have been thoroughly discussed and summarized by Ellis (1979), Perkins (1980), Buras (1980) and Reya (1981).

The most direct tests of the logarithmic QCD scale-breaking effects involve nonsinglet structure functions like $xF_3(x,Q^2)$, since they do not depend on the (unknown) distribution $g(x,Q^2)$ of the gluons in the nucleon. In this case the QCD predictions can be obtained by considering the change in the valence quark distribution $q_v(x,Q^2)$ due to an improvement in resolving power with increasing Q^2. In leading order of α_s it will be

$$\frac{\partial q_v(x,Q^2)}{\partial Q^2/Q^2} = \frac{\alpha_s(Q^2)}{2\pi} \int_x^1 \frac{dx'}{x'} P_{q\to q}\left(\frac{x}{x'}\right) q_v(x',Q^2) \qquad (2.5)$$

(Altarelli & Parisi 1977). Here, $P_{q\to q}(z)$ describes the probability that a quark has split into quark and gluon with momentum fractions z and 1-z, respectively. $P_{q\to q}(z)$ is calculable in QCD. Equation (2.5) shows that a precise measurement of the quark distribution or structure function at one value of Q^2 will allow to predict its behaviour for other Q^2 values, provided $\alpha_s(Q^2)$ is known.

A simple analytical prediction for the scaling violation can be obtained in terms of moments

$$M_n(Q^2) = \int_0^1 \frac{dx}{x} x^n q_v(x,Q^2) \qquad (2.6)$$

of the quark distribution or structure functions, because for moments the convolution in eqn.(2.5) reduces to a simple product. Defining a_n to be the n-th moment of the quark splitting function $P_{q\to q}(z)$, one obtains

$$\frac{d[\ell n\, M_n(Q^2)]}{d[\ell n\, Q^2]} = \frac{\alpha_s(Q^2)}{2\pi}\, a_n. \qquad (2.7)$$

Such an equation holds in any field theory. The Q^2 dependence of $\alpha_s(Q^2)$ is characteristically logarithmic for QCD while for fixed point theories (e.g. Abelian vector, or scalar gluons) it has a power behaviour. The constant a_n is proportional to the anomalous dimension d_n and depends on the spin of the field. For QCD it is given by

$$a_n = -\frac{33 - 2N_f}{6} \qquad d_n = -\frac{2}{3}\left[1 - \frac{2}{n(n+1)} + 4 \sum_{j=2}^{n} \frac{1}{j}\right] \qquad (2.8)$$

Equation (2.7) can be tested in two particularly clear ways. Because of

$$\frac{d[\ell n\, M_n(Q^2)]}{d[\ell n\, M_m(Q^2)]} = \frac{a_n}{a_m}\ , \qquad (2.9)$$

a plot of $\ell n\, M_n(Q^2)$ vs. $\ell n\, M_m(Q^2)$ must be linear in any field theory, with a slope given by the ratio of anomalous dimensions and thus characteristic of the spin of the gluon. For QCD, inserting eqn.(1.1) into (2.7) one obtains

$$M_n(Q^2) = A_n \left[\ell n \frac{Q^2}{\Lambda^2}\right]^{-d_n} \qquad (2.10)$$

where A_n is a constant that must be extracted from the data. This logarithmic Q^2 dependence of the moments is a crucial prediction of QCD; fixed point theories lead to a power law behaviour.

In Fig. 2.2 a plot of $\ell n\, M_n(Q^2)$ vs. $\ell n\, M_m(Q^2)$ is shown for two pairs of moments of xF_3. One set of data is from bubble chamber experiments (the Gargamelle heavy liquid bubble chamber at the CERN-PS and the BEBC chamber filled with Ne-H_2 at the SPS), combined by the Aachen-Bonn-CERN-London-Oxford-Saclay Collaboration (Bosetti et al. 1979).

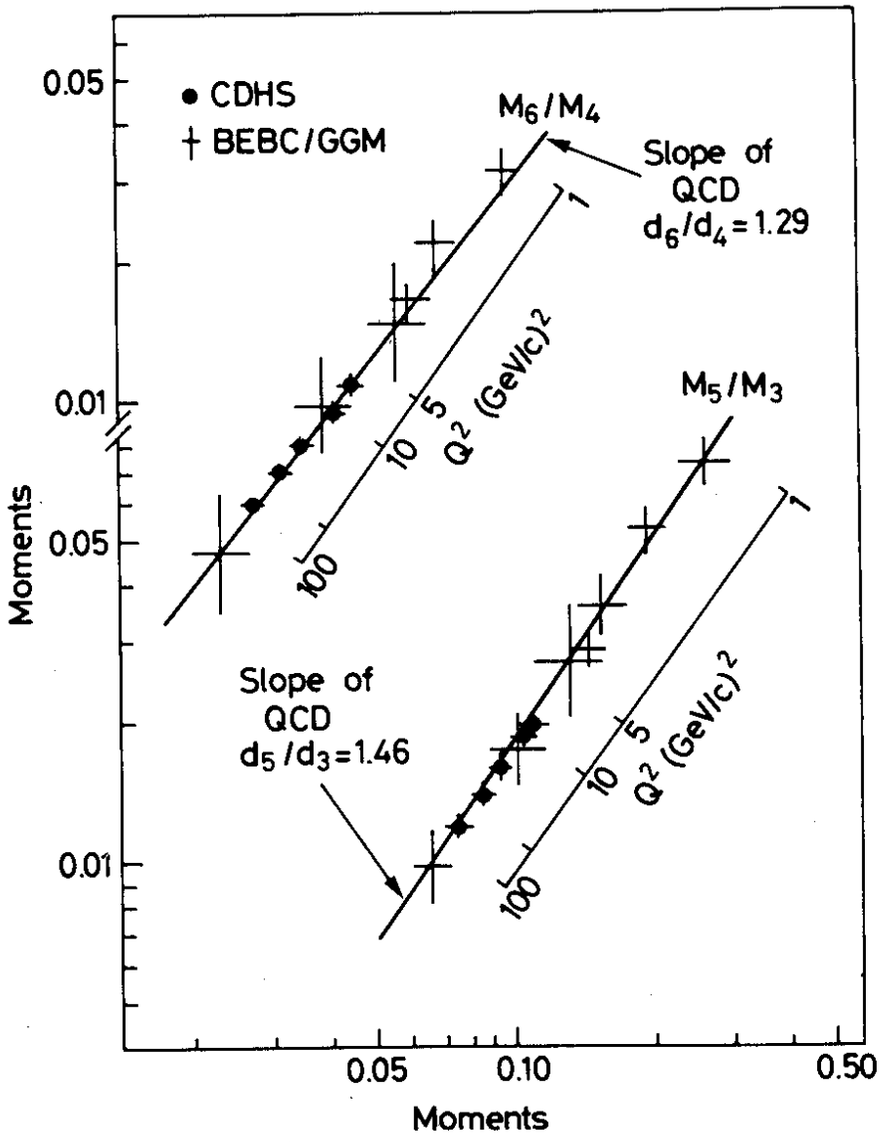

Fig. 2.2 Relations between Nachtmann moments of the structure function xF_3, from the Aachen-Bonn-CERN-London-Oxford-Saclay collaboration (Bosetti et al. 1979) using the bubble-chambers BEBC/GGM, and from the CERN-Dortmund-Heidelberg-Saclay counter neutrino experiment (de Groot et al. 1979) at CERN.

The other set of data is from the CERN-Dortmund-Heidelberg-Saclay (CDHS) counter neutrino experiment using an Fe target (de Groot et al. 1979), combined at low Q^2 and high x with electron-deuteron scattering data from MIT and SLAC (Atwood et al. 1976, Bodek et al. 1979). A linear relationship between the different moments is indeed seen. Moreover, the slopes are consistent with the ratios a_n/a_m given by QCD, as shown in Table 1. This is an important result. Several cautionary remarks on the moment determination are in order:

i) There are no measurements at large Q^2, small x, preventing the evaluation of the lower moments. In the higher moments, the high-x region gets strongly weighted; here, the corrections for experimental resolution effects are large. Furthermore, an extrapolation to x = 0 and x = 1 must be made.

ii) The moments of different order n are strongly correlated with one another in a given experiment. Therefore, the slopes for different pairs of moments (as e.g. in Table 1) do not provide statistically independent information.

iii) The bubble chamber data contain significant contributions from the region $Q^2 < 10$ GeV^2 where nonperturbative effects are likely to be important. The significance of the slopes from these data for the gluon spin determination is therefore questionable. Even in the higher-Q^2 data of the CDHS collaboration kinematical target mass effects are still important, as seen by comparing in Table 1 the Nachtmann moments (Nachtmann 1974) with the ordinary moments (eqn.2.6) where the former imply corrections for these low-Q^2 effects.

We conclude that the moment-moment correlation of Fig. 2.2 is indeed as expected in field theory although for the lower-Q^2 part the agreement may be fortuitous. Vector gluons are slightly favored over scalar gluons (see Table 1).

A test of the crucial logarithmic Q^2 dependence (eqn.2.10) of the moments is shown in Fig. 2.3. Here, the Nachtmann moments of xF_3 have been determined by the CDHS group (de Groot et al. 1979). The plot shows $M_n(Q^2)^{-1/d_n}$ vs. $\ell n\ Q^2$ for which QCD predicts, for each n, a straight line with intercept $\ell n\Lambda^2$. The lines in Fig. 2.3 are results

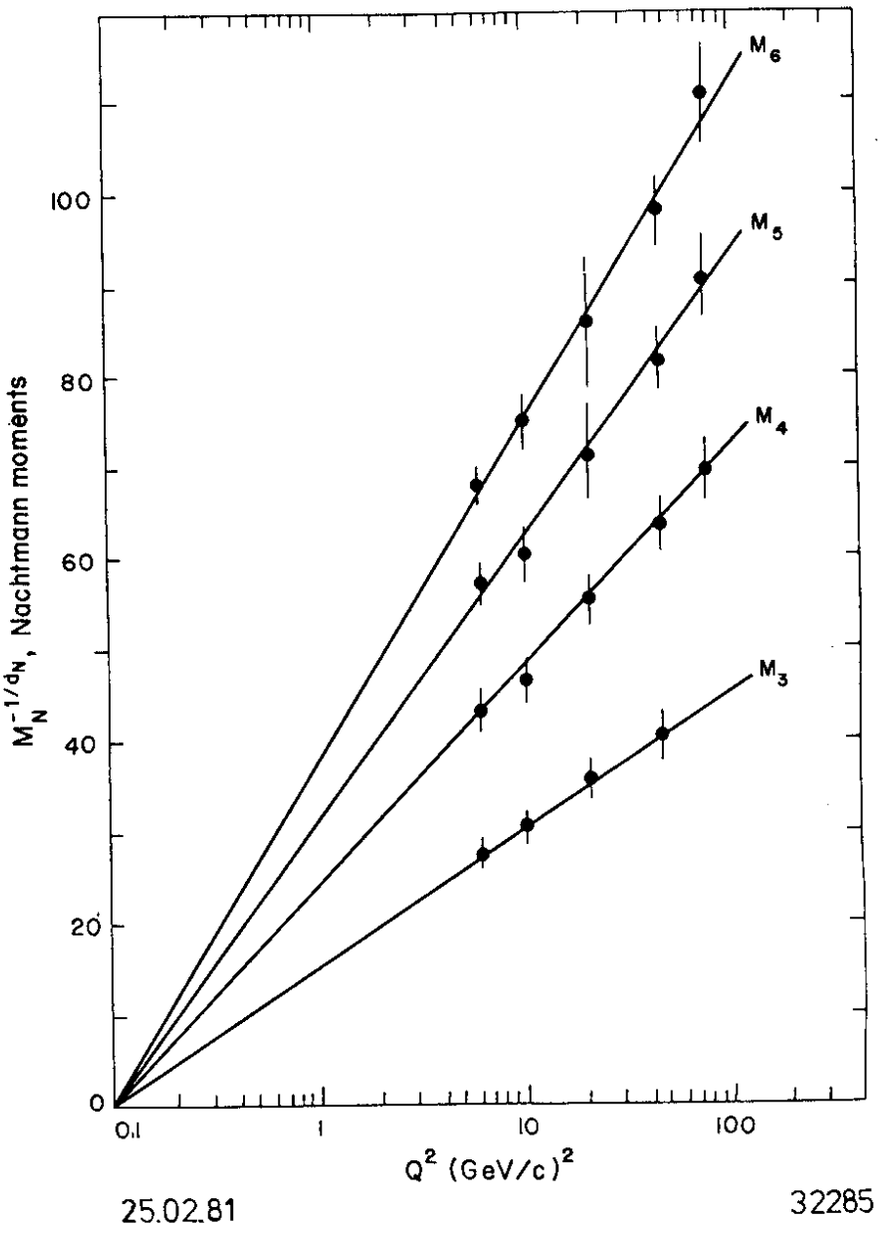

Fig. 2.3 Q^2 dependence of the Nachtmann moments of the structure function xF_3, from the CERN-Dortmund-Heidelberg-Saclay experiment at CERN (de Groot et al. 1979). The lines show the result of a fit of the leading-order QCD relation (2.10) to the data.

of a simultaneous straight-line fit to these moments; the fit describes the data well and gives, assuming $N_f = 4$ active flavours, the result $\Lambda = (0.33 \pm 0.10)$ GeV. An attempt to fit the moments by a power law violation of scaling between $Q^2 = 1$ and 10 GeV^2 does not seem to fit the data as well as the QCD logarithm (Ellis & Sachrajda 1979); however, fixed-point theories can not be ruled out on the basis of these moments (Reya 1979). A quantity more sensitive to discriminate QCD from other field theories, according to Glück and Reya (1979), is the $n = 2$ moment of a singlet structure function, e.g. the area under F_2. Of all field theories only QCD predicts this area to decrease when Q^2 rises, a tendency indeed supported by available data.

Although the moments allow a simple, clear-cut interpretation, a direct confrontation of the measured structure functions with QCD predictions has its own definite advantages. Among them are the avoidance of extrapolation into x regions where no data exist, the absence of large statistical correlations between the data points, and the possibility to clearly isolate kinematic regions where nonperturbative scale-breaking effects as discussed above (higher twist contributions, quark thresholds) or experimental uncertainties (resolution, assumptions on $R(x,Q^2)$, and radiative corrections) might be important. The QCD predictions are obtained by inverting the moments, or by solving the evolution equation (2.5) with a suitable parametrization of the quark distribution functions; the resulting structure functions can then be compared with the data, adjusting the value of Λ in the parametrization of $\alpha_s(Q^2)$ (Abbott & Barnett 1980, Baulieu & Kounnas 1979, Buras & Gaemers 1978, Gonzales-Arroyo et al. 1979, Martin 1979).

Results for $xF_3(x,Q^2)$ and $F_2(x,Q^2)$ from the CDHS neutrino experiment are shown together with a QCD fit in Fig. 2.4 (de Groot et al.1980). These data have improved statistics compared with the previously published ones (de Groot et al. 1979). Recall that the structure function F_2 has a singlet component (eqn.2.4) and that therefore the diagram of Fig. 2.1(d) contributes. This adds a term proportional to $P_{g\to q}(\frac{x}{x'})\ g(x',Q^2)$ in the evolution equation and requires an assumption on the x distribution $g(x,Q^2)$ of gluons in the nucleon. In extracting $F_2(x,Q^2)$ from the cross section data a constant $R(x,Q^2) = 0.1$ was used.

Both structure functions in Fig. 2.4 are seen to behave qualitatively similar, rising with Q^2 at small x and falling at large x (above x=0.3). The small-x data extend only to moderate Q^2. The increase with Q^2 in this region is more marked for F_2 than for xF_3. This is presumably due to the combined effect of the $q\bar{q}$ sea and the onset of charm production, both of which should not affect xF_3. In the large-x region the structure functions are strongly falling with increasing Q^2, particularly at the lower Q^2 values; this is a region possibly affected by higher order twist and target mass effects. (Note that at x = 0.7, Q^2 = 20 GeV^2 the total mass of all final state hadrons, including quark and target fragments, is only W = 3.1 GeV.) There is a region of intermediate x and Q^2 > 10 GeV^2 where the Q^2 dependence at fixed x is clearly indicative of a logarithmic fall, and is well described by the QCD fit. This leading order α_s fit to the data with Q^2 > 5 GeV^2 gives

$$\Lambda = 0.3 \pm 0.1 \text{ (statistic)} \pm 0.1 \text{ (systematic)} \text{ GeV}.$$

The fit was made to xF_3 for all x, and to F_2 for the valence-dominated (nonsinglet) region x > 0.4.

Results from other neutrino experiments than the ones discussed, although of less statistical power, have also shown scale breaking effects in the structure functions (Barish et al. 1978, Benvenuti et al. 1979, Sciulli 1980).

The structure function $F_2(x,Q^2)$ for charged leptons has been measured in a similar kinematic range as spanned by the neutrino data. In Fig. 2.5 the results of the Chicago-Harvard-Illinois-Oxford (CHIO) collaboration from muon proton scattering at FNAL are shown (Gordon et al. 1979), together with SLAC and SLAC-MIT electron proton data (Atwood et al. 1976, Bodek et al. 1979). In the extraction of F_2 from their data, the CHIO group assumed a constant $R(x,Q^2)$ = 0.52 equal to the average of their measurements over a restricted range of small x. Figure 2.6 presents results from the European Muon Collaboration (EMC) at CERN using an iron target; F_2 was evaluated under the assumption $R(x,Q^2)$ = 0.2 (Aubert et al. 1980). For comparison with the corresponding neutrino structure function one has to remember the weighting by the

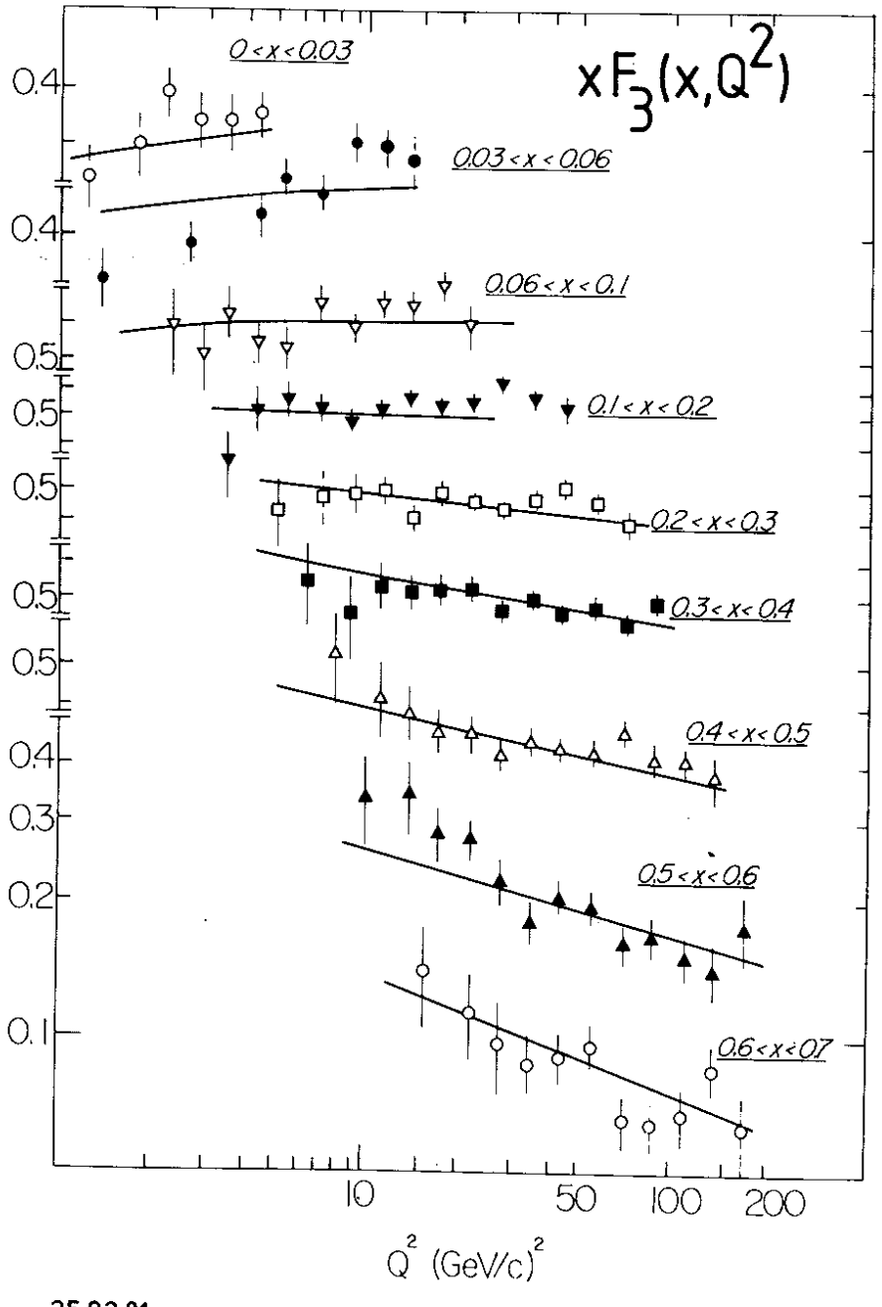

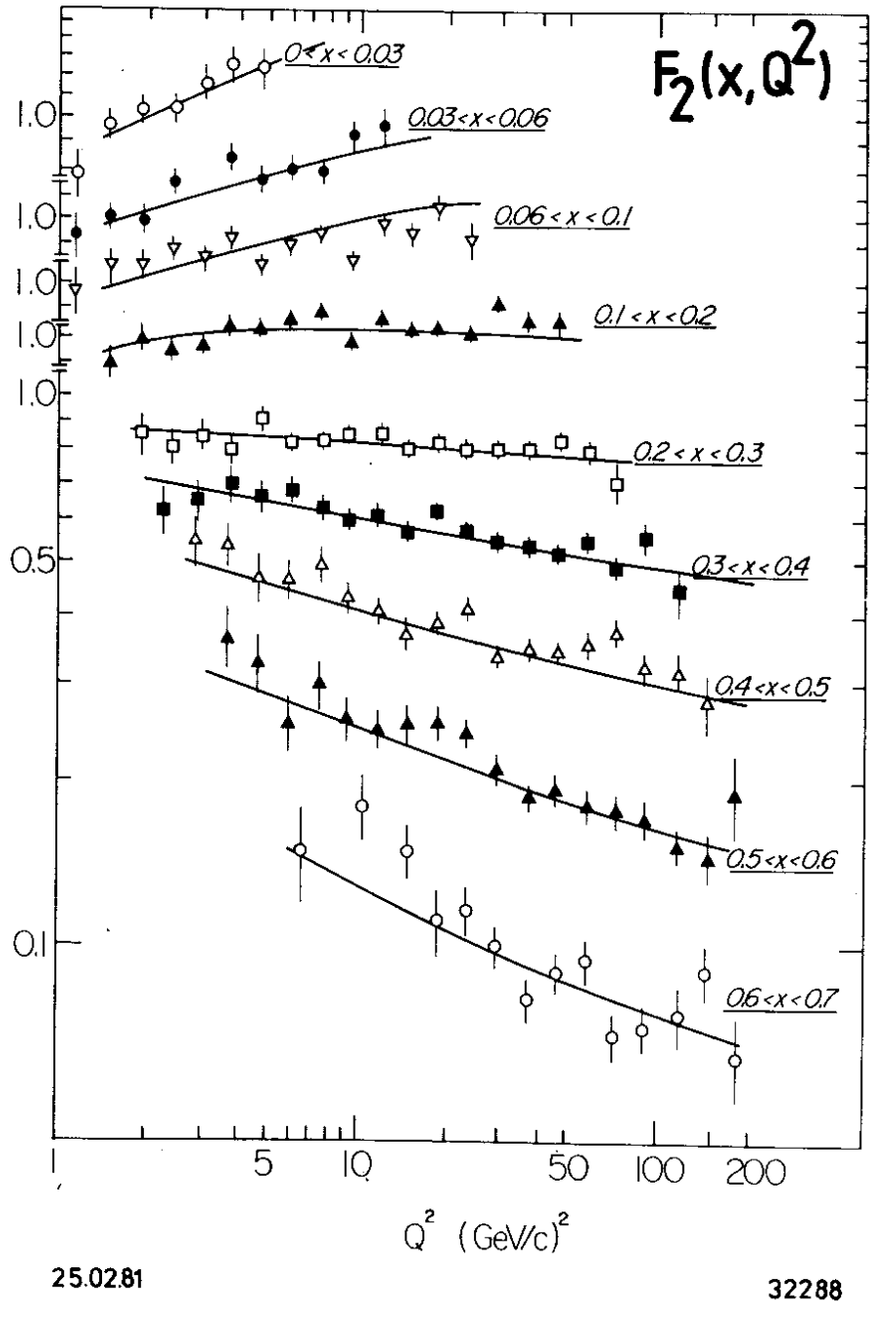

Fig. 2.4 The structure functions xF_3 and F_2 measured in the CERN-Dortmund-Heidelberg-Saclay neutrino experiment at CERN (de Groot et al. 1980). The lines show the result of a fit to the QCD evolution equations.

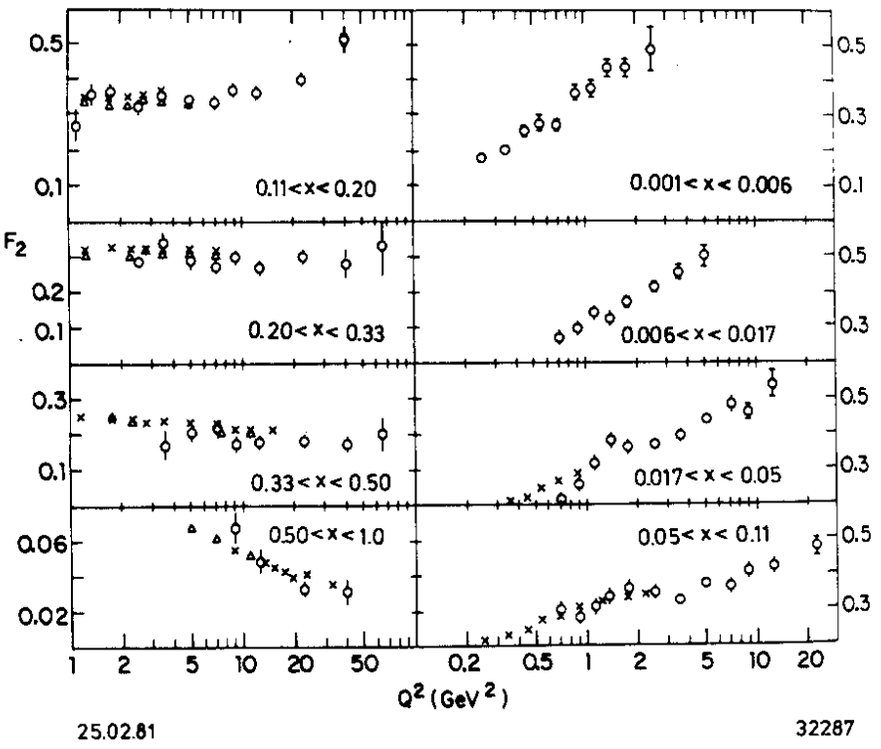

Fig. 2.5 The electromagnetic structure function F_2 from the Chicago-Harvard-Illinois-Oxford experiment at FNAL (Gordon et al. 1979, circles), combined with results from the SLAC and SLAC-MIT groups (Atwood et al. 1976, crosses, Bodek et al. 1979, triangles), showing scaling violations in the region $0.2 < Q^2 < 80$ GeV^2.

squared quark charges (a factor 5/18) and to note that the EMC muon data have been corrected for nuclear Fermi motion effects; taking these differences into account the muon and neutrino data are consistent with each other in overall normalization within their assigned errors (see, e.g. Sciulli 1980).

The electromagnetic structure function $F_2(x,Q^2)$ shows definite scaling violation which is smaller in the region of higher x than at low x. Part of this at low x can be explained by charm quark production (Aubert et al. 1980). The Q^2 dependence in the higher x region is slightly weaker than in the neutrino data; this difference can not be attributed to the Fermi motion effect and probably also not to assumptions on $R(x,Q^2)$ which affect the structure function mainly at low x.

QCD fits to these data can well describe the observed scaling violations. The quantitative results for Λ depend somewhat on the value of $R(x,Q^2)$ assumed and may be affected by higher twist and target mass effects operative at the lower Q^2 values. For the high-Q^2 experiment of EMC, a fit to the valence dominated range $0.25 < x < 0.65$ is shown by the curves in Fig. 2.6; the resulting value of Λ is

$$\Lambda = (0.10 \pm 0.10) \text{ GeV}$$

where the error includes systematic effects like uncertainty in $R(x,Q^2)$, Fermi motion corrections, and experimental resolution (Aubert et al. 1980). Fits to the lower-Q^2 data of Fig. 2.5 have generally tended to yield larger values of Λ (Gordon et al. 1979, Duke & Roberts 1980, Quirk et al. 1980).

Scale-breaking effects have also been observed in other muon scattering experiments at FNAL and CERN (Ball et al. 1979, Bollini et al. 1980). In particular, the Bologna-CERN-Dubna-München-Saclay collaboration (Bollini et al. 1980) has collected data with very high statistics at large Q^2; a preliminary analysis has shown only a very weak Q^2 dependence of F_2. The EMC group in addition to μ-Fe scattering has also measured μp scattering at high Q^2, with preliminary results on Λ being identical to those obtained with the Fe target (Aubert et al. 1980).

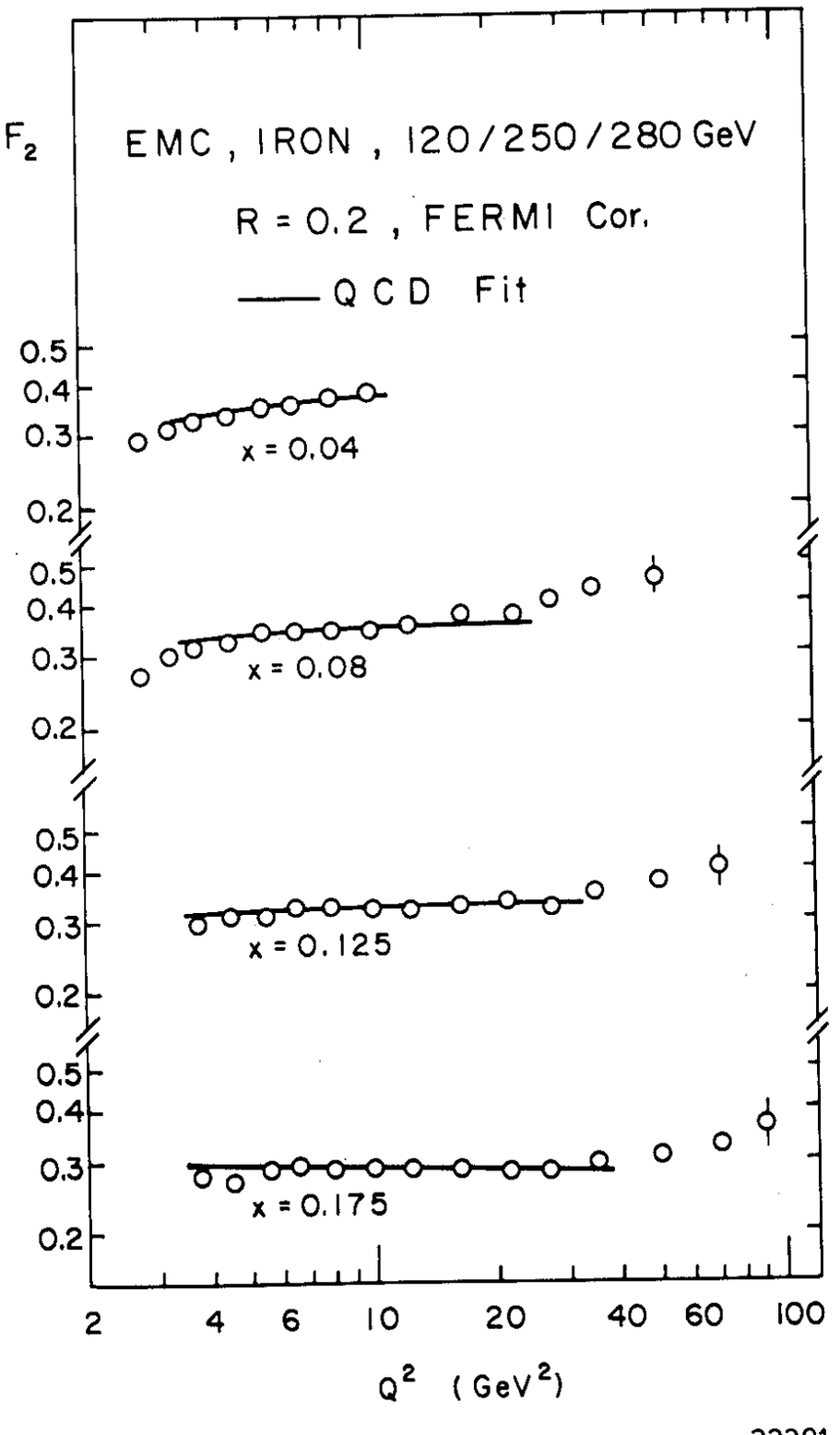

Fig. 2.6 a The electromagnetic structure function F_2 measured by the European Muon Collaboration at CERN (Aubert et al. 1980). The lines show the result of a fit to the QCD evolution equation. (The rise with Q^2 for $0.1 < x < 0.35$ at high Q^2 may be connected with radiative effects; it is not nearly as marked in the hydrogen target data of the same group.)

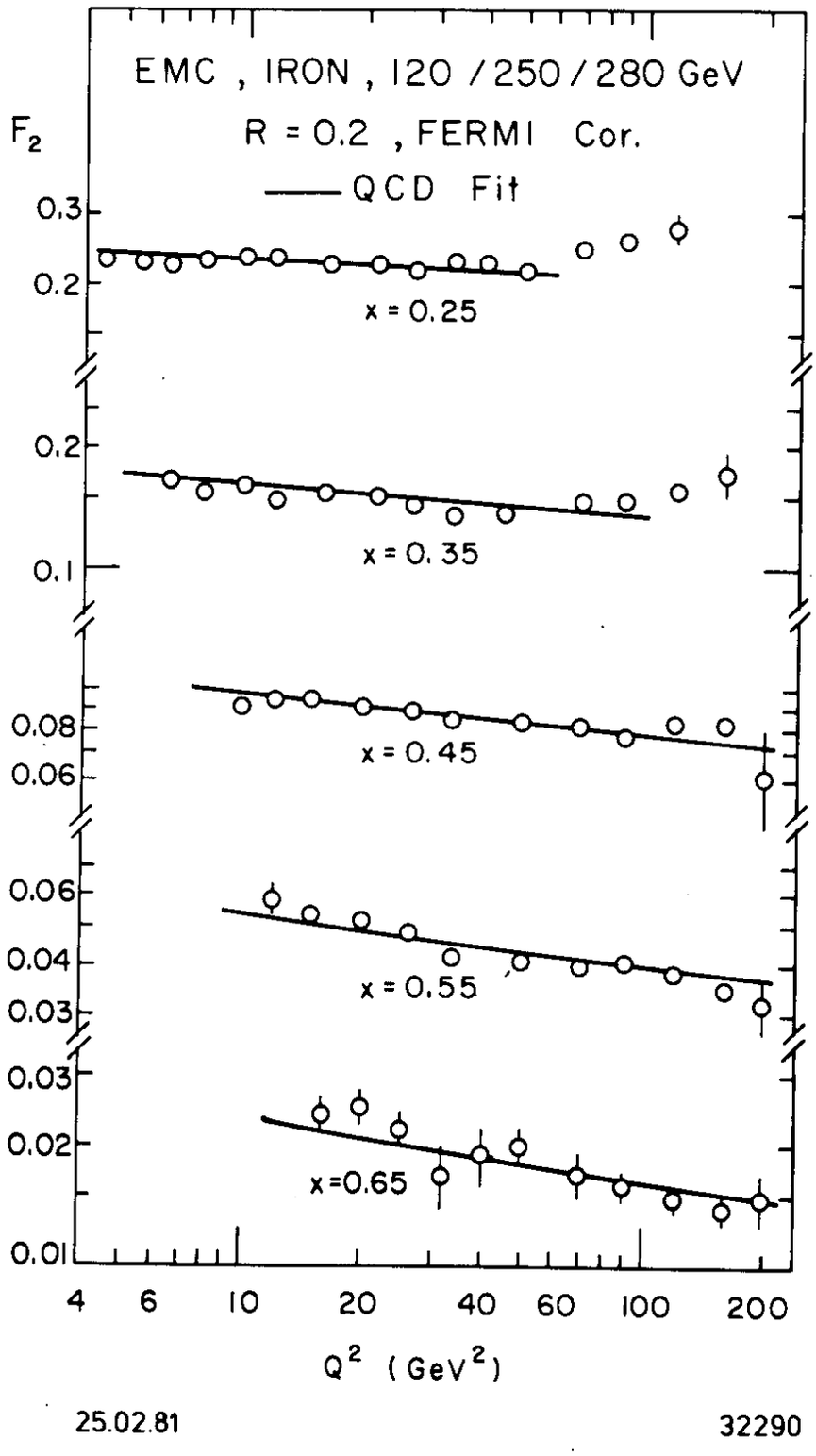

Fig. 2.6b same as Fig. 2.6a

The leading order QCD analyses that we have discussed so far imply the tacit assumption that the next-to-leading order α_s contributions can be neglected. Computations of these contributions have been made (for a review see Buras 1980). They are found to be large enough to be observable yet not so large as to completely invalidate the leading order predictions, Thus, the higher-order contributions will lead to deviations from the linear relationship of $\ell n M_n(Q^2)$ vs. $\ell n M_m(Q^2)$ (Fig. 2.2) and of $M_n(Q^2)^{-1/d_n}$ vs. $\ell n Q^2/\Lambda^2$ (Fig. 2.3). While the leading-order QCD formulae, although useful to fit data, yield values of Λ that have no well-defined relationship to those values extracted from other processes like e^+e^- annihilation (Bace 1978), in the next-to-leading order Λ can be meaningfully defined within a given renormalization convention. A sensitive way to search for the higher order effects is offered by a particular scheme that absorbs the next-to-leading order corrections to the moment $M_n(Q^2)$ into a redefinition of Λ such that the leading-order relationship (eqn.2.10) remains formally valid, however with higher order contributions causing the scale Λ to depend on n (Bardeen et al. 1978, Para & Sachrajda 1979). Data have been examined for these corrections and while there is no unambiguous evidence for them in the high-Q^2 region where target mass effects and higher twist contributions are small, the data are certainly not inconsistent with the higher order corrections (Buras 1980, Duke & Roberts 1980, Ellis & Sachrajda 1979, Gordon et al. 1979, Para & Sachrajda 1979, Quirk et al. 1980).

In summary, both the neutrino data on xF_3 and F_2 and the muon data on F_2 show scaling violations up to the highest Q^2 explored so far. QCD can well describe the Q^2 evolution of the structure functions. The size of the logarithmic scale-breaking effects, determined by $\alpha_s(Q^2)$ or, equivalently, Λ, is still uncertain mainly as a consequence of other scale-breaking effects that may be important in $Q^2 \lesssim 20$ GeV^2 and can cause the value of Λ extracted from the fits to depend on the kinematic region used. Nevertheless, an assumed uncertainty of Λ between, say, 0.05 and 0.5 GeV is equivalent to an uncertainty of $\alpha_s(Q^2)$ of only about a factor 2: for $N_f = 4$ at $Q^2 = 50$ GeV^2, α_s would lie between 0.15 and 0.28. A reliable and precise determination of Λ in deep-inelastic scattering will require either a firmer theoretical framework for the low-Q^2 behaviour, or an extension of the Q^2 range well beyond the present maximum values of about 200 GeV^2.

3. e^+e^- ANNIHILATION INTO HADRONS

3.1 The Total Cross Section

a) Experimental results

A precise measurement of the total cross section for e^+e^- annihilation into hadrons, σ_{tot}, offers a particularly clean test of QCD. Separation of the one photon annihilation events from hadronic events produced by two-photon scattering, which becomes increasingly important as the energy increases, is straightforward. It is achieved by demanding that the observed hadron energy exceeds a certain fraction of the total energy W. This cut eliminates also background from beam-gas scattering. Contamination from τ pair production is usually suppressed by a multiplicity and an effective mass cut. The acceptance efficiency of the high energy experiments is typically 70 - 80 % after all cuts are made. The luminosity is determined from small angle (few degrees) and/or large angle Bhabha scattering, $e^+e^- \to e^+e^-$. Sizeable corrections have to be applied for radiative effects such as photon emission in the initial state, vertex corrections and vacuum polarization (Bonneau & Martin 1971, Berends et al. 1974, 1980). The systematic uncertainties in acceptance, luminosity and radiative corrections are roughly of the same magnitude (typically 5 % each) and lead to a total systematic error of about ±10 %.

It is convenient to express σ_{tot} in units of the high energy $O(\alpha^2)$ cross section for μ pair production,

$$R = \sigma_{tot}/\sigma_{\mu\mu}$$
$$\sigma_{\mu\mu} = \frac{4\pi\alpha^2}{3s} \quad \left(= \frac{87.6}{s}\ \text{nb}, \quad s = W^2 \text{ in GeV}^2\right) \tag{3.1}$$

Fig. 3.1a shows R up to the highest energy measured at PETRA, W = 36.6 GeV. The error bars indicate only the statistical uncertainties. In order to reduce the statistical errors of the high energy data in Fig. 3.1b averages have been taken over the PETRA experiments (Timm1980, Cords 1980).

The τ contribution has been removed in all experiments. It should be noted that a contribution from pair production of a sequential charged

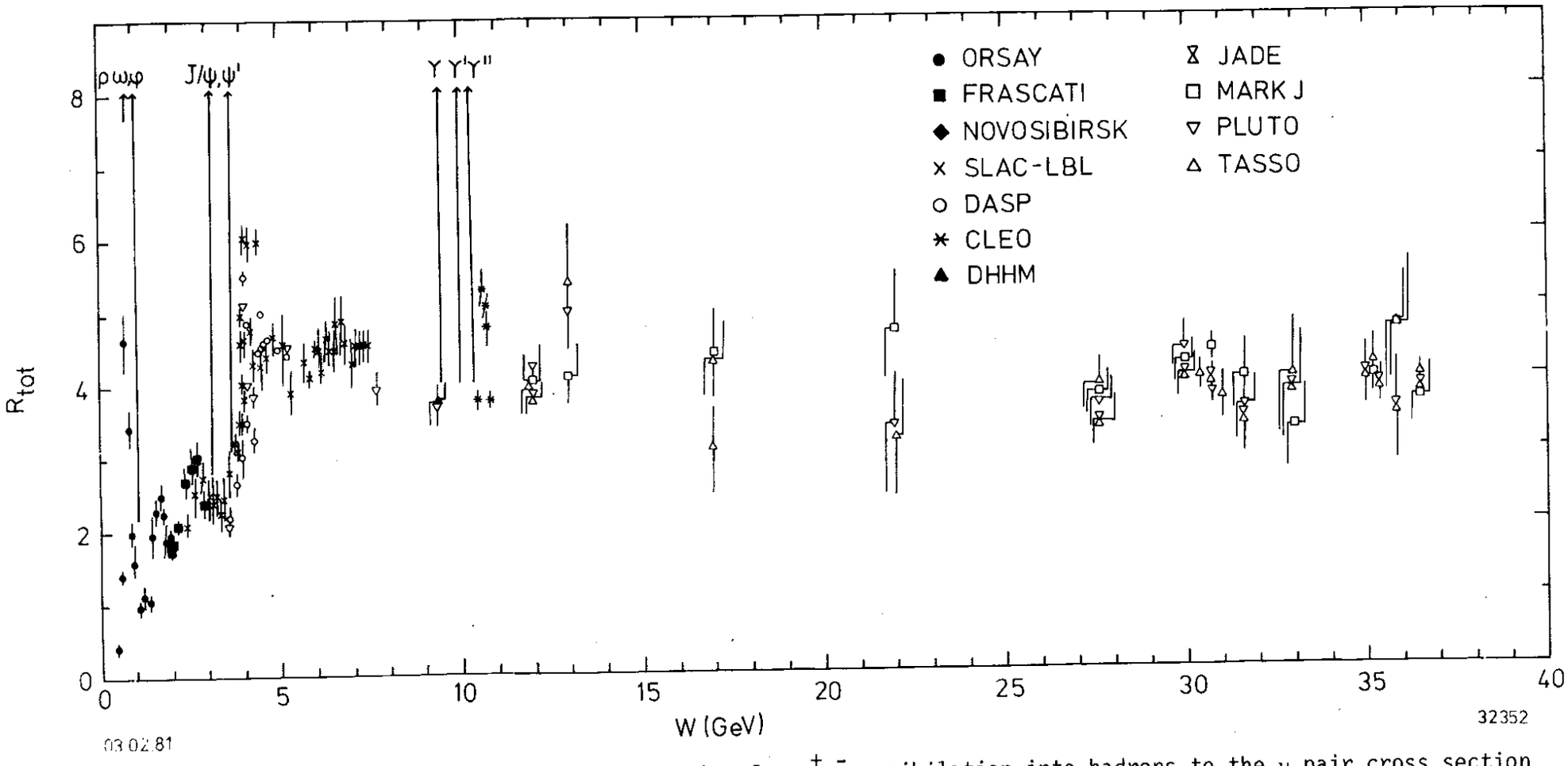

Fig. 3.1(a) The ratio R of the total cross section for e^+e^- annihilation into hadrons to the μ pair cross section $\sigma_{\mu\mu} = \frac{4\pi\alpha^2}{3s}$. (Quenzer 1977, Cordier et al. 1979, Sidorov 1976, Perez-Y-Yorba 1978, Schwitters 1976, Burmester et al. 1977, Brandelik et al. 1978a, Bacci et al. 1979, Berger et al. 1979a, Bartel et al. 1979 , Barber et al. 1979a, Bock et al. 1980, Brandelik et al. 1980a, Cords 1980).

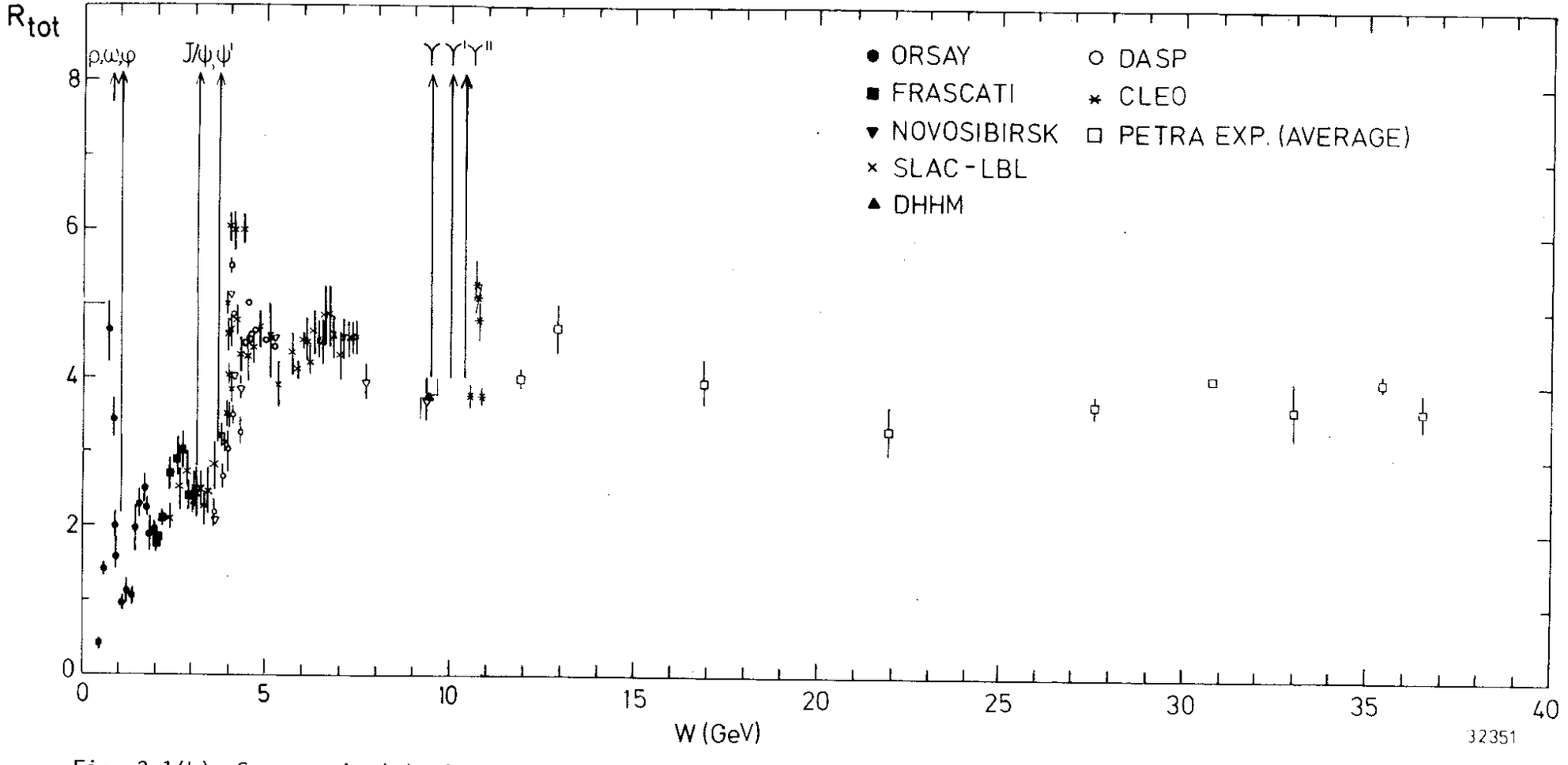

Fig. 3.1(b) Same as in (a) with averages taken over the PETRA data (energies $W \geq 12$ GeV).

lepton heavier than the τ is excluded by experiments at PETRA up to $W \simeq 35$ GeV (Barber et al. 1980a, Brandelik et al. 1980b, Berger et al. 1981, see also Cords 1980).

The outstanding features of R are spikes due to the excitation of vector states, ρ,..., and the fact that in between the families of vector states (ρ,...., J/ψ..., Υ,...) and above R is rather constant. The data above 1.5 GeV indicate two steps. Between 1.5 and 3.8 GeV R is approximately 2 - 2.5. Near charm threshold (at 4 GeV) R rises sharply to reach a new level around 4 which persists up to 36 GeV. This is in striking agreement with the quark parton model where e^+e^- annihilation into hadrons proceeds in two steps: first a pair of quarks is produced (Fig. 3.2a) which then fragment into hadrons. The total cross section

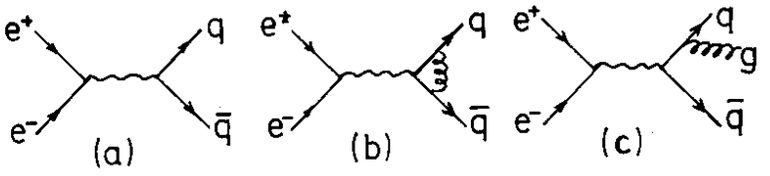

Fig. 3.2 Quark parton diagram and lowest order QCD diagrams for $e^+e^- \to q\bar{q}$.

is readily calculated. The cross section for producing a free $q\bar{q}$ pair is the same as for producing a $\mu^+\mu^-$ pair except that the quark charge e_q replaces the muon charge 1. Assuming that the produced $q\bar{q}$ pair turns into hadrons with unit probability one finds

$$R \equiv \sigma_{tot}/\sigma_{\mu\mu} = 3 \sum_{q=u,d,..} e_q^2 \qquad (3.2)$$

where the factor of three accounts for the fact that quarks come in three colours. Up to 3 GeV where only u,d and s contribute eq.(3.2) predicts R = 2. Above charm threshold R should rise to a level of 3.3. Beyond the Υ family the b quark contribution raises R to 3.7. The presence of the hypothetical t quark ($e_q = 2/3$) should manifest itself as a further step increasing R to R = 5. Both, the R measurements as

well as the analysis of the event shape exclude a possible t contribution up to W = 36 GeV (see Cords 1980).

The high energy data on R can be used to test whether quarks are pointlike, provided the quark parton picture is correct. In terms of the quark electric and magnetic formfactors G_E, G_M the ratio R is given by

$$R = 3 \sum e_q^2 \left\{ \frac{2m_q^2}{s} |G_E(s)|^2 + |G_M(s)|^2 \right\} \qquad (3.3)$$

where m_q is the quark mass and $m_q^2 \ll s$ has been assumed. If $G_E \sim G_M$ and all quarks have the same form factor we find:

$$R/R_o = |G_M(s)|^2 \qquad (3.4)$$

with $R_o = 3 \sum e_q^2$. With the ansatz

$$G_M(s) = (1 - s/M^2)^{-1} \qquad (3.5)$$

treating R_o as a free parameter and including the systematic uncertainties of σ_{tot} the data yield for $W \geq 17$ GeV, $M > 124$ GeV with 95% C.L. If quarks are composites of 3 subquarks G_M may have a dipole behaviour:

$$G_M(s) = (1 - s/M_D^2)^{-2} \qquad (3.6)$$

For this case the fit gives $M_D > 176$ GeV with 95 % C.L. Converting the M parameters into a length we conclude that quarks behave pointlike down to distances of $\sim 1 \cdot 10^{-16}$ cm.

b) Comparison with QCD

In QCD the quark parton result for R is modified:

$$R = 3 \sum_q e_q^2 \left[1 + \sum_{n=1}^{\infty} C_n \left(\frac{\alpha_s}{\pi} \right)^n \right] \qquad (3.7)$$

where quark masses have been put to zero.[2] The perturbation coefficients C_n have been computed up to second order (Dine & Sapirstein 1979, Chetyrkin et al. 1979, Celmaster & Gonsalves 1979). The first order coefficient $C_1 = 1$. The higher order coefficients depend on the normalization procedure. The preferred values are (see Barnett 1980, Llewellyn Smith 1980)

$C_2 = 1.99 - 0.12\ N_f$ $\quad\overline{MS}$ = minimal subtraction scheme

or $C_2 = -2.19 + 0.16\ N_f$ momentum space scheme.

After a careful examination of the theoretical problems at low energy ($W < 2$ GeV) Eidelman et al. (1979) deduced a rather small Λ value from the σ_{tot} data, $\Lambda \sim 0.1$ GeV. QCD fits to the intermediate energy region between 4 and 7 GeV have been presented by Barnett et al. (1980). We compare the QCD expression to the data measured above 20 GeV. This is an energy region which is well above heavy quark thresholds; furthermore higher twist effects should be negligible. The individual experiments yield as an average over $20 < W < 36$ GeV (Cords 1980):

$\overline{R}$ =	3.84 ± 0.10	JADE
	4.17 ± 0.10	MARK J
	3.82 ± 0.14	PLUTO
	4.00 ± 0.13	TASSO

A 10 % systematic uncertainty has to be added.
The average over all high energy data gives

$$\overline{R} = 3.97 \pm 0.06\ (\text{stat}) \pm 0.4\ (\text{syst}) \text{ for } \overline{W} = 33 \text{ GeV}.$$

The systematic uncertainty prevents an accurate determination of α_s. The data are in agreement with the perturbative expression and an extraction of α_s yields $\alpha_s = 0.24 \pm 0.06$ (stat) ± 0.26 (syst) or $\alpha_s = 0.30 \pm 0.07$ (stat) $^{+\ 0.7}_{-\ 0.3}$ (syst) depending on whether the first or the second expression for C_2 is used. Despite the large uncertainties

---

2) Corrections for finite quark masses have been calculated for R (Schwinger 1973) and for α_s (Georgi & Politzer 1974). If $\Lambda = 0.2$ GeV is assumed the mass corrections reduce α_s by 10 - 15 % in the region of interest ($W = 15$-40) GeV while R is changed by less than 1 %.

it follows from these values of α_s that the second order contribution to R is smaller than the first order one, i.e. $C_2(\alpha_s/\pi)^2 < \alpha_s/\pi$, suggesting that the perturbative calculation is reliable.

3.2 The Upsilon and the Three-Gluon Decay

a) Decay width

The direct decays of heavy quark-antiquark states, $Q\bar{Q}$, into light hadrons in QCD proceed by annihilation into gluons (Appelquist & Politzer 1975). For vector states V such as J/ψ or T the lowest order intermediate state has three gluons since one gluon is forbidden by colour and two by angular momentum conservation.

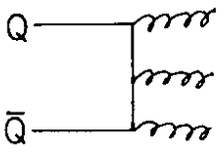

Fig. 3.3 QCD diagram for J/ψ or T decay into three gluons.

In the nonrelativistic approximation assuming the gluons turn into hadrons with unit probability the decay width is given by

$$\Gamma(V \to ggg \to \text{hadrons}) = \frac{160}{81}(\pi^2-9)\alpha_s^3 \frac{|\psi(0)|^2}{M^2}$$

where M is the vector meson mass. The $Q\bar{Q}$ wave function at the origin, $\psi(0)$, can be eliminated by comparison with the decay width into lepton pairs:

$$\Gamma(V \to e^+e^-) = 16\pi\alpha^2 e_Q^2 \frac{|\psi(0)|^2}{M^2} \tag{3.9}$$

which leads to

$$\frac{\Gamma(V \to ggg \to \text{hadrons})}{\Gamma(V \to e^+e^-)} = \frac{10}{81}\frac{\pi^2-9}{\pi}\frac{\alpha_s^3}{e_Q^2\alpha^2} \tag{3.10}$$

This expression is obtained in leading order QCD. The first order QCD corrections modify $\Gamma(V \to ee)$ by a factor $(1 - \frac{16}{3\pi}\alpha_s)$ (Barbieri et al.1975).

Since the next order corrections for $\Gamma(V \to \text{hadrons})$ are unknown we prefer to use eq.(3.10). In Table 2 the α_s values determined from the J/ψ and Υ parameters are shown. For $\Gamma(V \to ggg \to \text{hadrons})$ the width for direct decay of V into hadrons was used:

$$\Gamma_{dir} = \Gamma_{tot} - \Gamma(V \to \gamma X) - (N_\ell + R)\Gamma(V \to ee) \qquad (3.11)$$

where N_ℓ is the number of different lepton pairs V can decay into, and $R = \sigma_{tot}/\sigma_{\mu\mu}$ off resonance. The ratio of the α_s values, $r = \alpha_s(\Upsilon)/\alpha_s(J/\psi) = 0.89 \pm 0.23$ may be compared to the prediction of eq.(1.1), $r = 0.81$ for $\Lambda = 0.1$ GeV and $r = 0.54$ for $\Lambda = 1$ GeV. Either value is compatible with the data.

Since the direct decays are supposed to proceed via a three gluon intermediate state we expect hadrons from Υ direct decays to emerge in three jets. Consequently, the final states produced in Υ decays should differ markedly from the two-jet structure observed off resonance. In case of the J/ψ the available c.m. energy is too low to test for a three-jet structure: the average particle momentum is only 0.4 GeV/c.

b) Gluon energy spectrum and event configuration in $\Upsilon \to ggg$

We mention some of the properties expected for three gluon decay (Koller & Walsh 1977, Brodsky et al. 1978, Fritzsch & Streng 1978, DeRujula et al. 1978, Koller et al. 1979). The energy spectrum for (massless) gluons in terms of their fractional energies $x_i = 2E_i/M$ is given by

$$\frac{1}{\Gamma}\frac{d^2\Gamma}{dx_1 dx_2} = \frac{1}{\pi^2 - 9}\left\{\left(\frac{1 - x_3}{x_1 x_2}\right)^2 + \left(\frac{1 - x_2}{x_3 x_1}\right)^2 + \left(\frac{1 - x_1}{x_2 x_3}\right)^2\right\} \qquad (3.12)$$

Integration over x_2 yields the single gluon distribution

$$\frac{1}{\Gamma}\frac{d\Gamma}{dx} = \frac{2}{\pi^2 - 9}\left\{\frac{x(1 - x)}{(2 - x)^2} + \frac{2 - x}{x} + 2\left[\frac{1 - x}{x^2} - \frac{(1 - x)^2}{(2 - x)^3}\right]\ln(1-x)\right\} \qquad (3.13)$$

The most probable configuration is one where two of the three gluons

share almost all of the available energy. Of course, such a configuration will produce nearly two-jet events. The gluon

Fig. 3.4 Most probable configuration for $\Upsilon \to 3g$ decay.

momenta lie in a plane. The scaled energies are directly related to the angles Θ_i between the gluon directions (see Fig. 3.5).

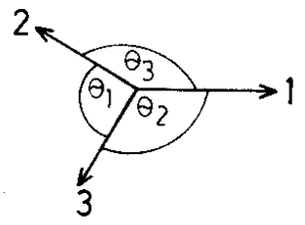

Fig. 3.5 Schematic diagram for the $\Upsilon \to 3g$ decay.

$$x_i = \frac{2\sin\Theta_i}{\sin\Theta_1 + \sin\Theta_2 + \sin\Theta_3} \qquad (3.14)$$

We may ask for the probability to observe three well separated jets: in 38 % of the events the three gluons are emitted within $\pm 20^0$ of the symmetric configuration ($\Theta_i = 120^0$), i.e. smallest angle between any pair of gluons is 80^0.

The orientation of the three-gluon configuration in space can be described in terms of Θ and β, the angles of the most energetic gluon and of the normal to the three gluon plane, measured with respect to the beam axis:

$$W(\cos\Theta) = 1 + 0.39\ \cos^2\Theta \qquad (3.15)$$

$$W(\cos\beta) = (1 - \tfrac{1}{3}\cos^2\beta). \qquad (3.16)$$

For scalar gluons the Θ distribution would be (Koller and Krasemann 1979)

$$W(\cos\Theta) = 1 - 0.995\ \cos^2\Theta \qquad (3.17)$$

c) Jet measures

The jet structure of the final hadron states is commonly studied in terms of sphericity S (Bjorken & Brodsky 1970) and/or thrust T (Brandt et al. 1964, Fahri 1977):

$$S = 3/2\ (\Sigma P_{Ti}^2)/(\Sigma P_i^2) \qquad 0 \leq S \leq 1 \tag{3.18}$$

$$T = \Sigma |P_{\parallel i}|/\Sigma P_i \qquad 0.5 \leq T \leq 1 \tag{3.19}$$

where the P_i are the total particle momenta, and P_{Ti}, $P_{\parallel i}$ are the transverse and longitudinal particle momenta relative to the jet axis, which is chosen such that ΣP_{Ti}^2 ($\Sigma |P_{\parallel i}|$) is minimal (maximal) for sphericity (thrust). Sphericity measures approximately the square of the jet cone half opening angle ($\langle\delta\rangle \equiv \langle P_T/P_{\parallel}\rangle$), $S \approx 3/2\ \langle\delta^2\rangle$. Extreme two jettiness ($\delta = 0$) leads to $S = 0$ and $T = 1$ while for spherical events S approaches 1 and T approaches 0.5. Both, S and T have their particular merits: sphericity being proportional to the square of the transverse momentum is more sensitive to changes in the P_T distribution. Thrust is linear in the particle momenta. Therefore T is unaffected by splitting of momenta as it happens in fragmentation or particle decays (Sterman & Weinberg 1977, Fahri 1977).

The topology from Υ decay has been studied in terms of the triplicity. Triplicity, T_3, is a generalization of thrust and is defined as follows (Brandt & Dahmen 1979): Group particle momentum vectors $\vec{p}_i$ into three nonempty classes C_1,C_2 and C_3 with total momenta $\vec{p}(C_\ell) = \sum_{i\in C_\ell} \vec{p}_i$. The triplicity is then obtained by taking all possible permutations and maximizing the sum of the moduli $|\vec{p}(C_3)|$:

$$T_3 = \text{Max} \left\{ |\vec{p}(C_1)| + |\vec{p}(C_2)| + |\vec{p}(C_3)| \right\} / \sum P_i \tag{3.20}$$

The values of T_3 vary between $T_3 = 1$ for a perfect three-jet event and $T_3 = 3\sqrt{3}/8 = 0.65$ for a spherical event. The jet directions are given by the $\vec{p}(C_\ell)$. The jets are then ordered such that $|\vec{p}(C_1)| \geq |\vec{p}(C_2)| \geq |\vec{p}(C_3)|$.

d) Models for quark and gluon fragmentation

At very high energies quark and gluon jets may be pictured as pencil beams of particles which are well isolated in space. At presently available energies the fragmented particles spread out and cause overlap between jets. An infrared stable way to define and measure jets in QCD has been introduced by Sterman and Weinberg (1977). In this procedure the jet cross section is defined for suitable chosen cuts on the jet energy and opening angle. It is equivalent to the technique used in QED to deal with bremsstrahlung in the infrared limit and is expected to lead to finite results in perturbative QCD. Unfortunately, at available energies the effects of hadronization cannot be neglected. Therefore detailed fragmentation models have been used to unfold the primary parton distributions from the observed particle distributions. At the same time the models allowed to evaluate the corrections for detector effects. In most analyses, the framework of Field and Feynman (1978) was used to describe the fragmentation of quarks into hadrons. The fragmentation process is treated as a recursive cascade in which a quark radiates mesons. The process is characterized by several parameters:

(i) a_F. The primordial fragmentation function $f^h(z)$ of a quark into a hadron h, $q \to q' + h$ is taken to be

$$f(z) = 1 - a_F + 3a_F(1 - z)^2, \quad z = \frac{(P_{\parallel} + E)_h}{(P_{\parallel} + E)_q} \tag{3.21}$$

a_F is assumed to be the same for u,d,s quarks, for c and b: a_F=0. (see e.g. Bjorken 1978).

(ii) σ_q. The distribution of the transverse momentum q_T of the quarks in the jet cascade is assumed to be $\sim\exp(-q_T^2/2\sigma_q^2)\, dq_T^2$

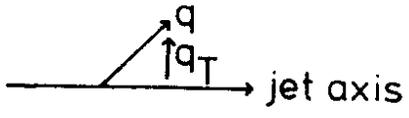

Fig. 3.6 Quark transverse momentum.

(iii) P/(P+V). Only pseudoscalar (π,K,..) and vector mesons (ρ,K^*,..) are assumed to be produced. P/V is the ratio of pseudoscalar to vector mesons produced in the primordial cascade.

(iv) $q\bar{q}$ pairs are generated from the vacuum with the probability $u\bar{u} : d\bar{d} : s\bar{s} = 2 : 2 : 1$.

Field & Feynman (1978) found that a satisfactory description of the available data could be obtained with $a_F = 0.7$, $\sigma_q = 0.25$ GeV/c and P/(P+V) = 0.5. A recent analysis of high energy e^+e^- jet production (Brandelik et al. 1980c) yielded rather similar values, $a_F = 0.57 \pm 0.20$, $\sigma_q = 0.32 \pm 0.04$ GeV/c and P/(P+V) = 0.56 ± 0.15.

Different assumptions have been used to describe gluon fragmentation. For example

(i) the gluon fragments via $g \rightarrow q\bar{q}$ by imparting its whole momentum to one of the two quarks (Hoyer et al. 1979);

(ii) the two quarks share the gluon momentum according to the Altarelli-Parisi (1977) splitting function (Ali et al. 1980):

$$f(z) = z^2 + (1 - z)^2 \qquad z = E_g/E_q.$$

The quarks then turn into hadrons as described above.

The fragmentation process is incorporated in elaborate Monte Carlo programs (Hoyer et al.1979, Ali et al.1979,1980) which can be used to simulate the detector, impose the same selection criteria as used in the analysis of the real data, and account for radiative effects (Berends & Kleiss 1980).

e) Experimental results

Fig. 3.7 shows σ_{tot} in the vicinity of the Υ as measured at DORIS (Berger et al. 1978, Darden et al. 1978, Bienlein et al. 1978). Comparison of the final states below and at the resonance reveals a dramatic change in event shape. The two-jet structure dominant off resonance disappears on resonance. This is best seen from the energy dependence of the average sphericity <S> in Fig. 3.8. At low energies, $W \lesssim 4$ GeV, the observed <S> values are close to those predicted by a

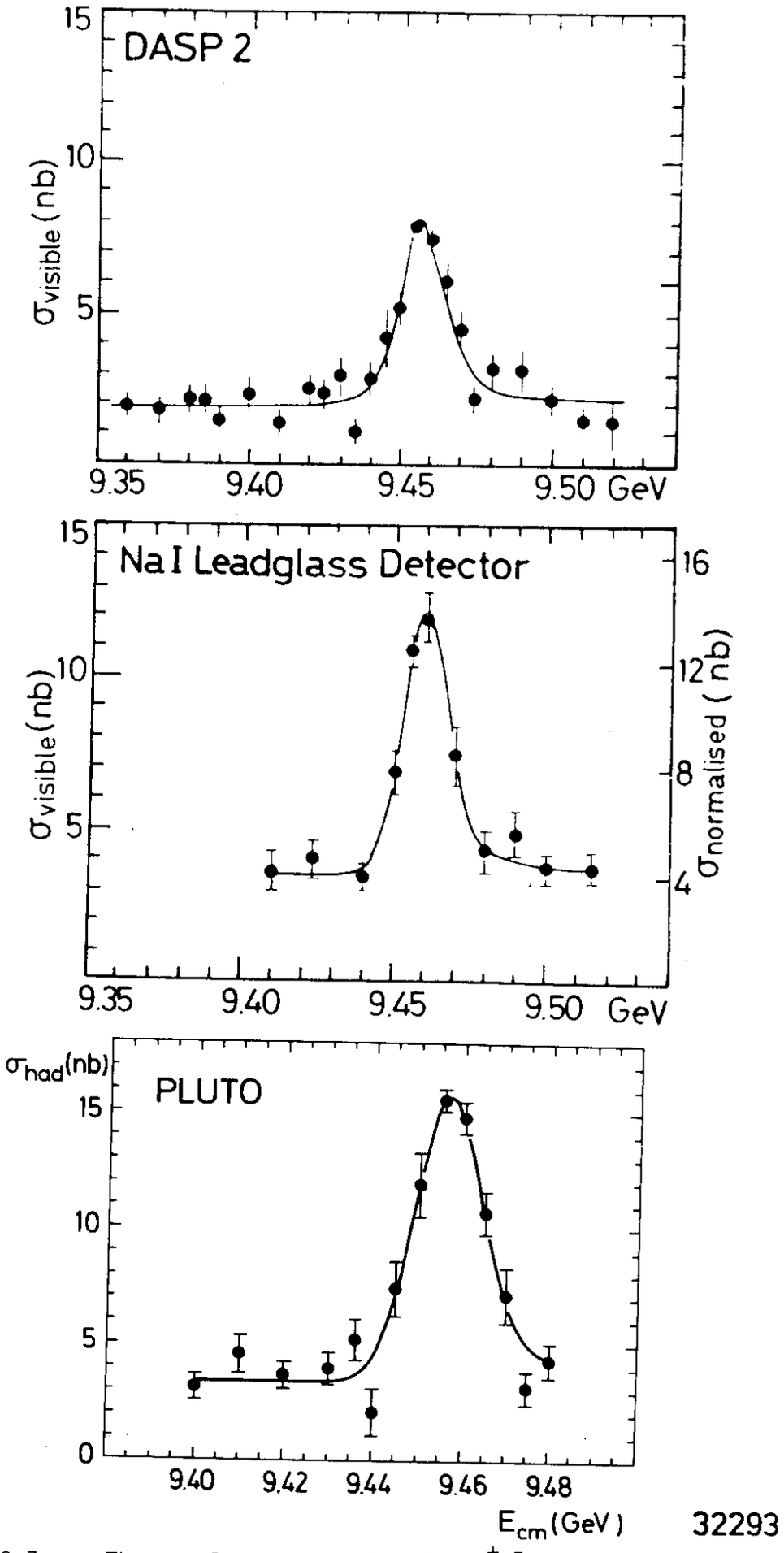

Fig. 3.7 The total cross section for e^+e^- → hadrons in the vicinity of the T (Darden et al. 1978, Bienlein et al. 1978, Berger et al. 1978).

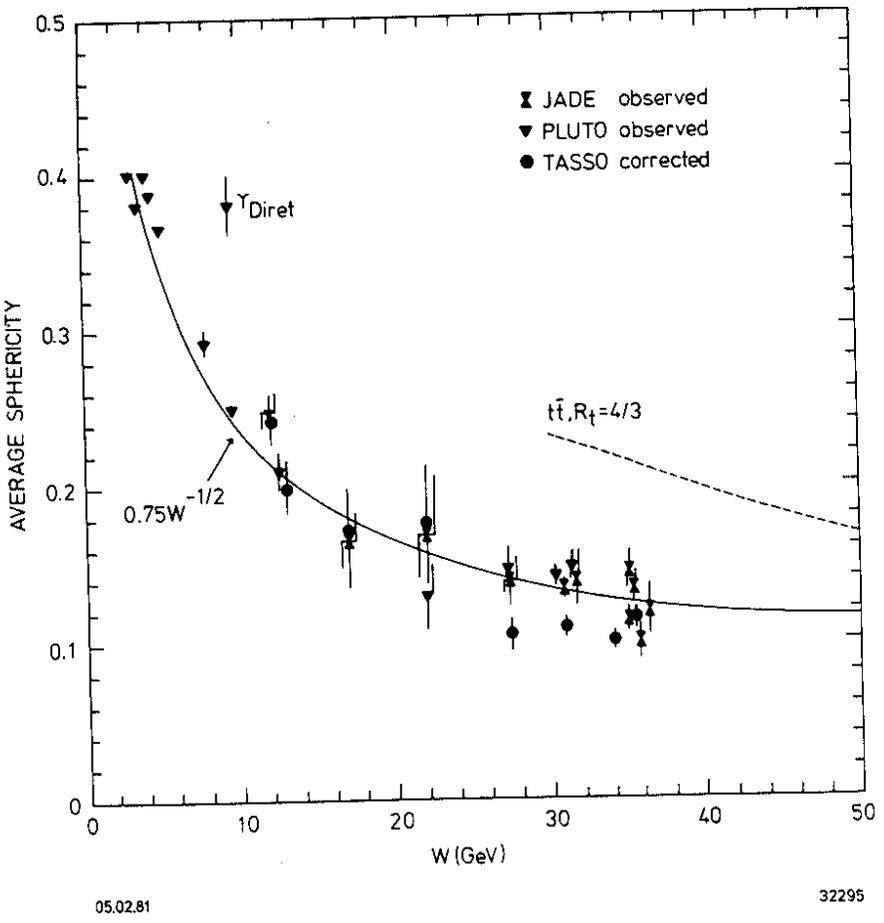

Fig. 3.8 The average sphericity as measured by the JADE, PLUTO and TASSO groups (see Cords 1980).

pure phase space distribution, $\langle S \rangle \approx 0.4$. Above 5 GeV, $\langle S \rangle$ decreases rapidly with increasing W; the particles become more and more collimated. The jet cone angle $\langle \delta \rangle$ shrinks from $\sim 31^{\circ}$ at W = 4 GeV to 17° near 36 GeV. Events from Υ decay on the other hand have a large average sphericity, $\langle S \rangle \approx 0.4$, a value close to the prediction for phase space.

A detailed analysis of the event shapes from Υ decay was presented by the PLUTO group (Brandt 1979, Berger et al. 1980a). Three processes contribute to events in the Υ region, the direct hadronic decay, the decay through the one-photon channel and the nonresonant continuum:

$$\sigma_{on} = \sigma_{dir} + \sigma_{1\gamma} + \sigma_{cont} \tag{3.23}$$

$\sigma_{1\gamma}$ can be related to σ_{cont} using the rate of μ pairs observed on and off the resonance leading to

$$\sigma_{dir} = \sigma_{on} - \sigma_{cont} \frac{\sigma_{\mu\mu}^{on}}{\sigma_{\mu\mu}^{off}} \tag{3.24}$$

The value measured for $\sigma_{\mu\mu}^{on}/\sigma_{\mu\mu}^{off}$ is 1.24 ± 0.22. The total number of events available for the analysis were 1781 on resonance and 442 in the continuum (near W = 9.4 GeV). The latter events were used to determine by proper subtraction the distributions for the direct decays of the Υ. The study included charged particles and neutrals (i.e. photons). The data shown below are uncorrected. The model predictions to be shown include the effects of acceptance and initial state radiation. The thrust distributions (Fig. 3.9) show the distinctly different behaviour of the Υ direct decays (Υ_{direct}) and of the off resonance region. The off resonance data prefer high T values or a two-jet structure while the on resonance distribution peaks at lower T values. The model for quark pair production, $e^+e^- \rightarrow q\bar{q}$, describes the off resonance data rather well (see curve) but fails for Υ_{direct}. Phase space may be considered as the opposite extreme to two-jet production. In Fig. 3.9 the Υ_{direct} data are compared to two versions of phase space, one where only pseudoscalars (π,K) are generated and one where pseudoscalars and vectors (ρ,K^*) are generated in equal proportion. The two versions predict similar T distributions. They reproduce the trend of the data but fail to give a quantitative description by many standard deviations. On average the predicted thrust is lower than observed.

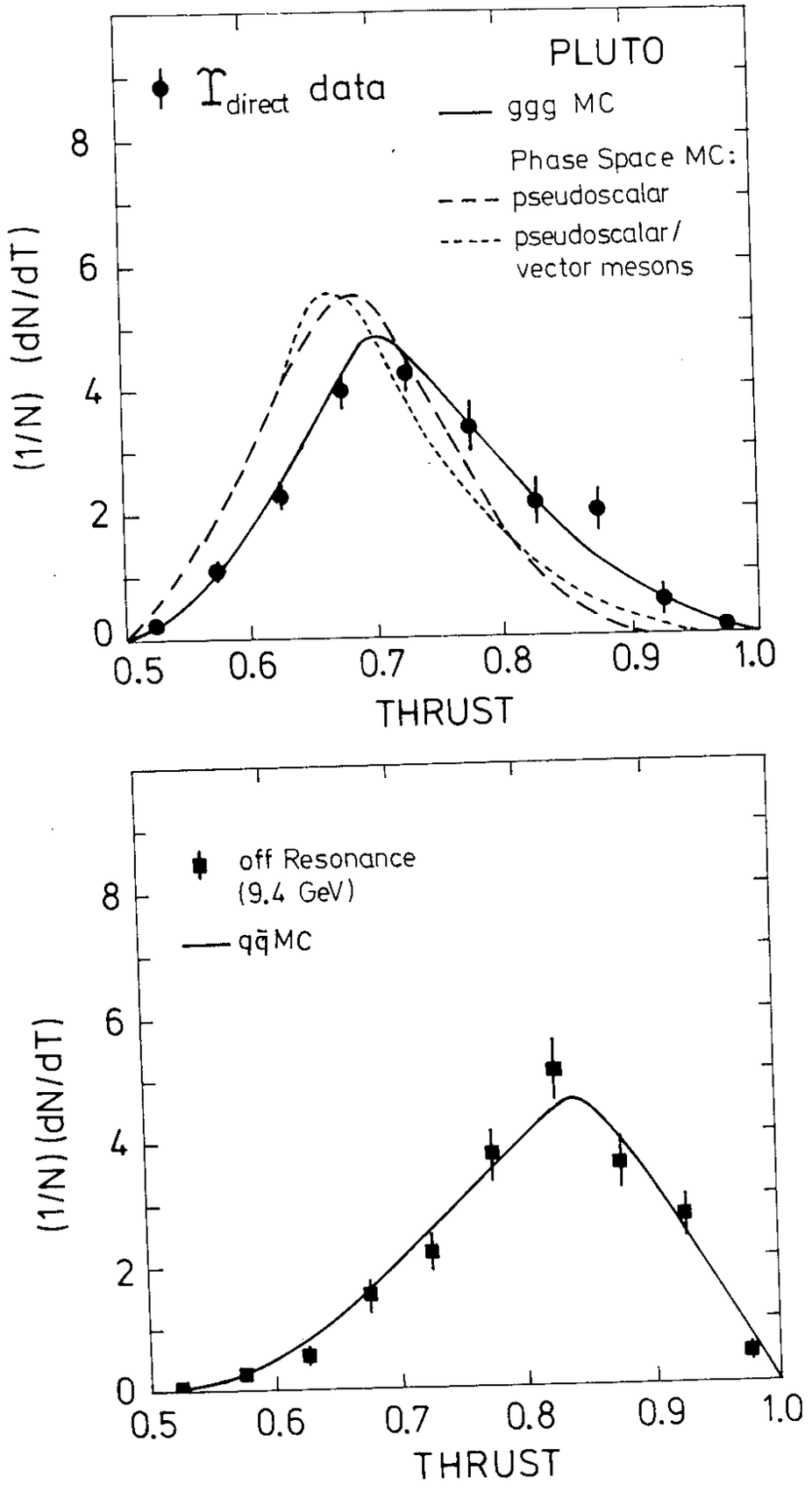

Fig. 3.9 Distribution of thrust for Υ-direct decays and off-resonance events. The curves show fits with a three gluon model and for phase space models with only pseudoscalar and pseudoscalars plus vector particles. From the PLUTO group (Ch.Berger et al. 1980a).

The three-gluon decay distribution supplemented with a Monte Carlo calculation of gluon fragmentation is also shown in Fig. 3.9. It is seen to fit the resonance data well.

The Υ events where searched for a three-jet structure using the triplicity method. The procedure was tested with Monte Carlo events generated according to $\Upsilon \to ggg$. Defining $\delta_1, \delta_2, \delta_3$ to be angles between the original gluon directions and the reconstructed triplicity axes the test yielded $<|\cos\delta_1|> = 0.78$, $<|\cos\delta_2|> = 0.71$ and $<|\cos\delta_3|> = 0.53$. No correlation means $<|\cos\delta|> = 0.5$. Clearly, only the two most energetic jets can be reconstructed with some reliability. This is a consequence of the comparatively low mass of the Υ.

For the sake of comparison between the on and off resonance region the triplicity analysis has been applied in both regions. Fig. 3.10 shows the distribution of Θ_3, the angle between the two most energetic jets for on and off resonance events. As expected, off resonance the two most energetic jets are almost anticollinear ($\Theta_3 = 180^0$). On resonance the average angle is considerably smaller, $\Theta_3 \approx 150^0$. The conclusion is the same as drawn from the analysis of thrust: the Υ direct data do not show two-jet structure; they are not fit by phase space; they are well reproduced, however, by the three-gluon model as shown by the curves in Fig. 3.10. Similar conclusions have been reached by the LENA group (Niczyporuk et al. 1981b).

As mentioned before the angular distribution of the most energetic gluon with respect to the beam axis is sensitive to the gluon spin. Fig. 3.11 shows the LENA data for the most energetic jet together with the predictions for scalar and vector gluons. The data disagree with the scalar prediction while they are consistent with vector gluons.

The Υ data lead to several conclusions:

1. The event structure is inconsistent with the two-jet model. This excludes the possibility of colourless gluons (Walsh & Zerwas 1980). If they would exist the Υ would decay via a single gluon intermediate state (the dominant process in this case) into a pair of light quarks, $\Upsilon \to g \to q\bar{q}$ giving rise to two-jet events.

2. The data disagree with a phase space like behaviour. They are also inconsistent with decay into three scalar gluons.

3. The data are well described by the QCD prediction of Υ decaying into three vector gluons, $\Upsilon \rightarrow ggg$.

No attempt has yet been made to identify the exclusive final states reached from Υ decay or produced off resonance. A comparison between the two cases should provide interesting information on the differences between quark and gluon fragmentation. There are two pieces of data that bear on this question. The average charged particle multiplicity $\langle n_{CH} \rangle$ for Υ direct decays is found to be larger than off resonance, viz.

$$\langle n_{CH} (\Upsilon_{dir}) \rangle = 8.2, \qquad \langle n_{CH}(off) \rangle = 7.6.$$

However, this does not imply that a gluon of given energy produces more charged particles in the fragmentation process than a quark; a similar increase e.g. would be expected if the Υ would decay into three quarks. To see this, assume $\langle n_{CH} \rangle$ for a quark jet of energy E_{jet} to be given by one half of $\langle n_{CH} \rangle$ observed in e^+e^- annihilation at energy $W = 2\, E_{jet}$. From the average jet energies of 4.1, 3.4 and 2.0 GeV measured in Υ decay (Berger et al. 1980a) one then expects (Hanson 1978, Niczyporuk et al. 1981b):

$$\langle n_{CH} (\Upsilon_{dir}) \rangle = 8.0, \qquad \langle n_{CH}(off) \rangle = 7.6$$

which is in accord with the observations. The analysis of the inclusive particle spectra of the DASP II group (Schmidt-Parzefall 1980) shows that Υ_{direct} decays yield a factor of two more protons (antiprotons) per event than off-resonance production. It is interesting to note that a similar observation has been made by the DASP group (Brandelik et al. 1978b) for the J/ψ.

3.3 Three-Jet Production in the Continuum

a) Transverse momentum distributions

The data from hadron scattering suggested a Gaussian P_T distribution for quark fragmentation into hadrons,

$$d\sigma/dp_T^2 \sim \exp(-p_T^2/2\sigma_q^2) \qquad (3.25)$$

The parameter σ_q for pions was measured to be of the order of 0.25 GeV/c almost independent of the reaction energy. Deviations from a simple Gaussian behaviour were observed at high energies and large P_T values (see e.g. Darriulat 1980). The e^+e^- annihilation data from SPEAR (Hanson 1978) and DORIS (Berger et al. 1980b) at energies up to 10 GeV were found to be consistent with an energy independent σ_q around 0.3 GeV/c. (For a review see Wiik & Wolf 1979). With the advent of PETRA higher energies became available and a rapid broadening of the P_T distribution with increasing c.m. energy was observed (Cashmore 1979). It was found to be correlated with the production of planar events some of which showed a definite three-jet structure (Söding 1979, Brandelik et al. 1979b, Barber et al. 1979b, Berger et al. 1979b, Bartel et al. 1980). The occurrence of three-jet events due to hard gluon bremsstrahlung had actually been predicted by Polyakov (1975), Ellis et al. (1976), De Grand et al. (1977), Hoyer et al. (1979), Kramer et al. (1978, 1979, 1980).

In discussing the experimental evidence, we begin by showing in Fig. 3.12 the transverse momentum distribution $1/\sigma_{tot}\ d\sigma/dP_T^2$ evaluated with respect to the sphericity axis for three regions of total c.m. energy W between 12 and 36 GeV (Brandelik et al. 1979b, 1981b). The broadening of the P_T^2 distribution with rising energy is clearly borne out by the data. The 12 GeV distribution is well fitted by the $q\bar{q}$ two-jet model assuming σ_q = 0.3 GeV/c. To fit the high energy distribution with the same model, σ_q had to be increased to 0.45 GeV/c.

In Fig. 3.13 the average P_T and P_T^2 values are shown as a function of c.m. energy W. Above 12 GeV both $\langle P_T \rangle$ and $\langle P_T^2 \rangle$ rise with W; the increase is most pronounced in $\langle P_T^2 \rangle$. The observed behaviour lead to a

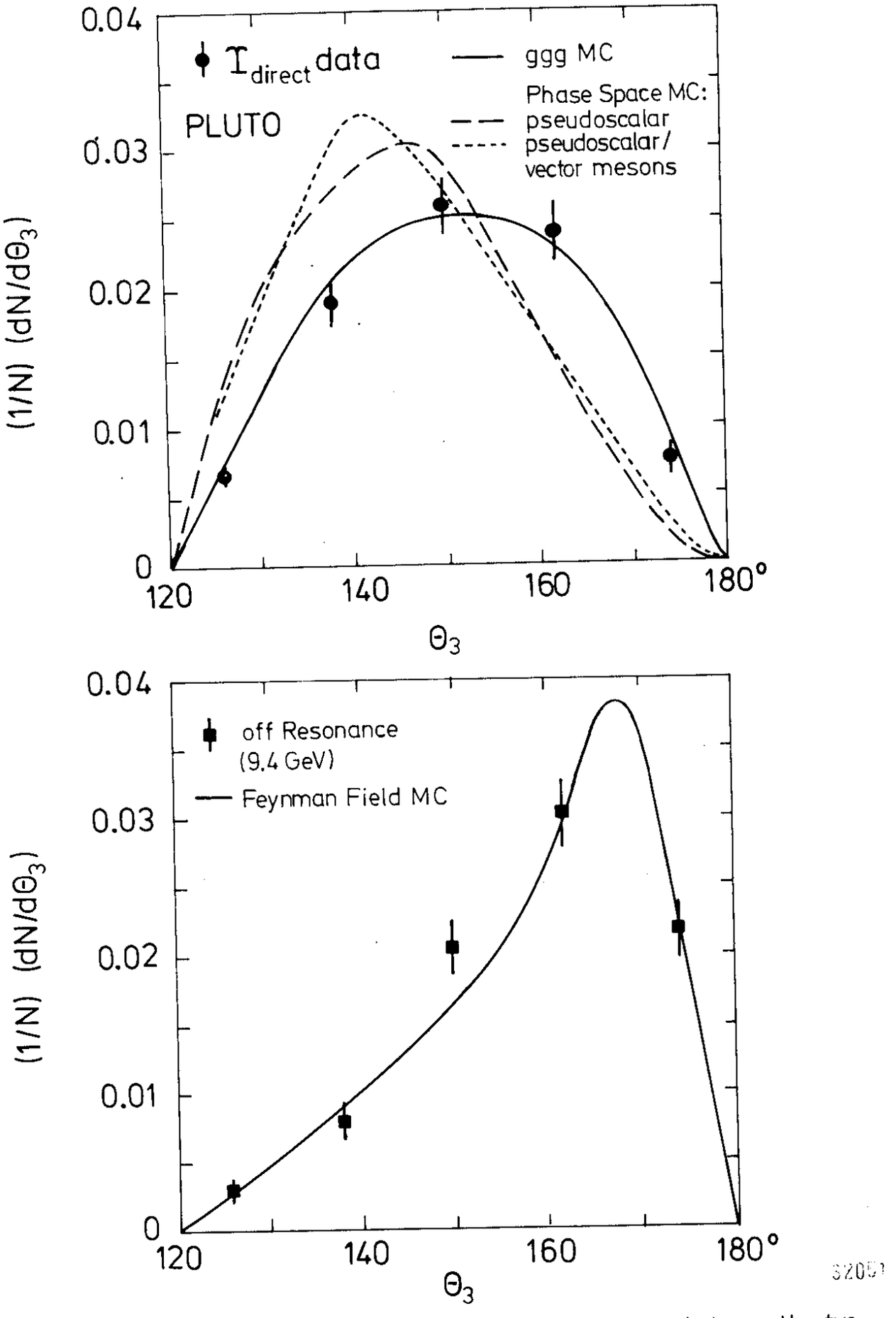

Fig. 3.10 Distribution of the reconstructed angle Θ_3 between the two most energetic jets for Υ-direct decays and off resonance events. The curves are explained in Fig. 3.9. From the PLUTO group (Ch.Berger et al. 1980a).

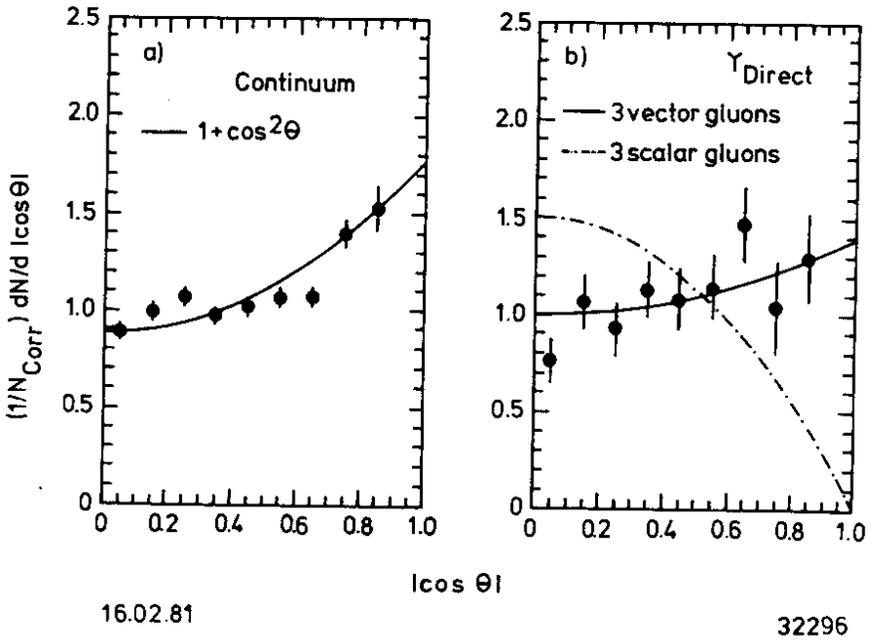

Fig. 3.11 Angular distribution of the thrust axis for off-resonance events and T-direct decays. The curves for the T direct data show the predictions for vector and scalar gluons. From the LENA group (Niczyporuk et al. 1981b).

detailed analysis of the event shapes. If it was caused by an energy dependence of σ_q the events would still possess a two-jet structure but the diameter of the "cigar" in terms of $\langle p_T^2 \rangle$ will increase with energy (see Fig. 3.14).

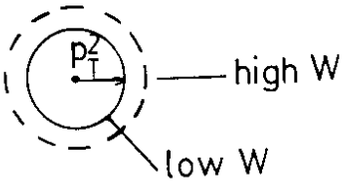

Fig. 3.14 Illustration of the P_T^2 distribution around the jet axis.

QCD predicts an increase in the average P_T^2 through gluon bremsstrahlung. In lowest order this leads to the process $e^+e^- \to q\bar{q}g$ described by diagram c in Fig. 3.2. Quark, antiquark and the gluon span a plane in the total c.m. system. Provided all three partons have sufficient energy and the gluon was emitted under a large angle the hadrons resulting from fragmentation tend to lie close to a common plane. Denoting by x_1, x_2 the fractional energies of the quarks, $x_i = 2E_i/W$, the cross section for gluon emission (diagrams 3.2(c)) is given by (Ellis et al. 1976, De Grand et al. 1977):

$$\frac{d\sigma(q\bar{q}g)}{dx_1\, dx_2} = \frac{2\alpha_s}{3\pi}\, \sigma_o\, \frac{x_1^2 + x_2^2}{(1-x_1)(1-x_2)} \qquad (3.26)$$

where $\sigma_o = 3\sigma_{\mu\mu} \sum e_q^2$. The infrared singularity in the integrated version of eq.(3.26) cancels exactly against that arising from the interference of diagrams (a) and (b) in Fig. 3.2. The energy and angular distribution of the radiated gluon is equal to that of bremsstrahlung photons. For small gluon energies k

Fig. 3.15 Illustration of the process $e^+e^- \to q\bar{q}g$.

$$\frac{d\sigma(q\bar{q}g)}{dk\, d\Theta} \sim \frac{\alpha_s}{k \sin\Theta} \qquad (3.27)$$

From diagrams (a) - (c) of Fig. 3.2 the average transverse momentum $\langle k_T \rangle$ of the gluon relative to the momentum direction of the most energetic quark is found to grow almost linearly with energy:

$$\langle k_T \rangle \sim \alpha_s \cdot W \sim W/\ln W \qquad (3.28)$$

The curve in Fig. 3.13 shows the QCD prediction for the energy dependence of $\langle P_T^2 \rangle$ made prior to the measurements (Hoyer et al. 1979). It describes the trend of the data well.

If k_T is large compared to the typical transverse momentum σ_q in the fragmentation of a quark, the event will have a three-jet topology. Detection of the gluon jet requires high c.m. energies for two reasons. Firstly, at low energies gluon and quark jets overlap. Secondly, at low energies α_s is large such that multigluon emission becomes important and perturbative QCD will eventually fail.

Various methods have been proposed to study event shapes and to search for three jet structure (Nowak & Schiller 1975, Wu & Zobernig 1979, Brandt & Dahmen 1979, Babcock & Cutkosky 1980, Lanius 1980, Daum et al. 1980, Dorfan 1981). A basic tool to study event shapes has also been the momentum tensor (Bjorken & Brodsky 1970).

b) Momentum tensor

For each event one constructs from the measured particle momenta the second rank tensor M:

$$M_{\alpha\beta} = \sum_{j=1}^{N} P_{j\alpha} P_{j\beta} \qquad (\alpha,\beta = x,y,z) \qquad (3.29)$$

Let $\hat{n}_1$, $\hat{n}_2$ and $\hat{n}_3$ be the unit eigenvectors of this tensor associated with the eigenvalues Λ_1, Λ_2 and Λ_3 which are ordered such that $\Lambda_1 < \Lambda_2 < \Lambda_3$. Note that

$$\Lambda_i = \sum_j (\vec{p}_j \vec{n}_i)^2 \qquad (3.30)$$

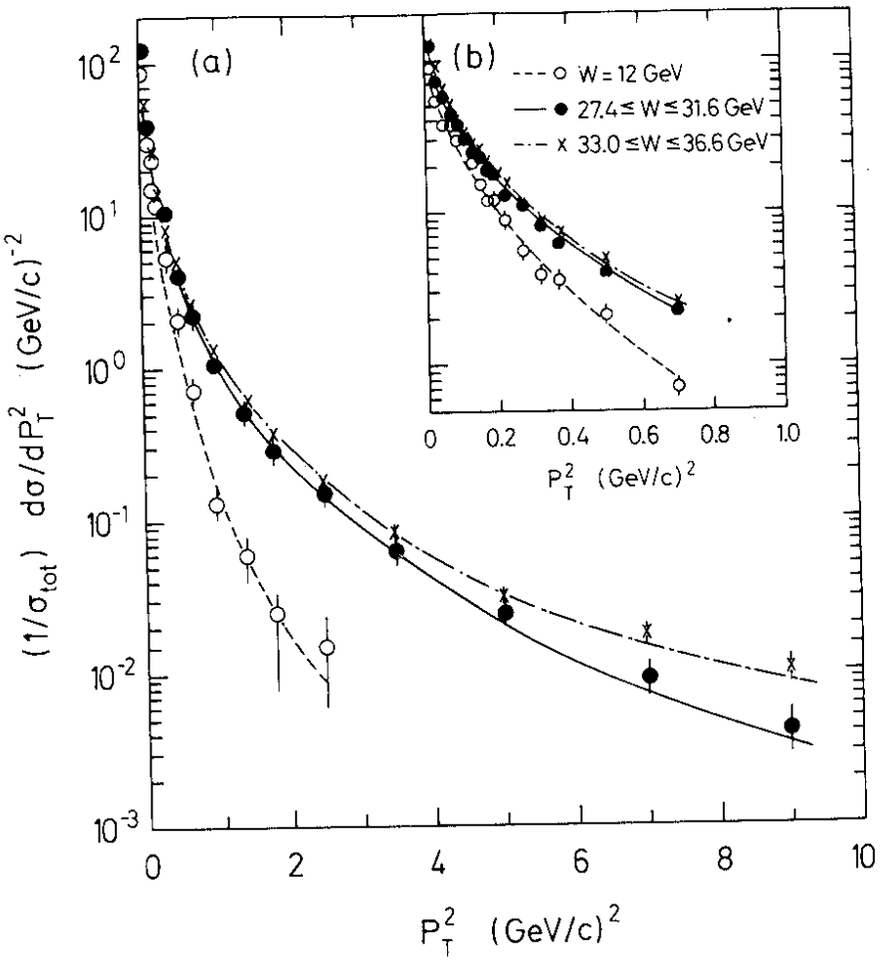

Fig. 3.12 Distribution of the square of the transverse momentum of charged particles with respect to the jet axis at 12, 27.4 - 31.6 and 35 - 36.6 GeV as measured by the TASSO group (Brandelik et al. 1979b, Brandelik et al. 1981b).

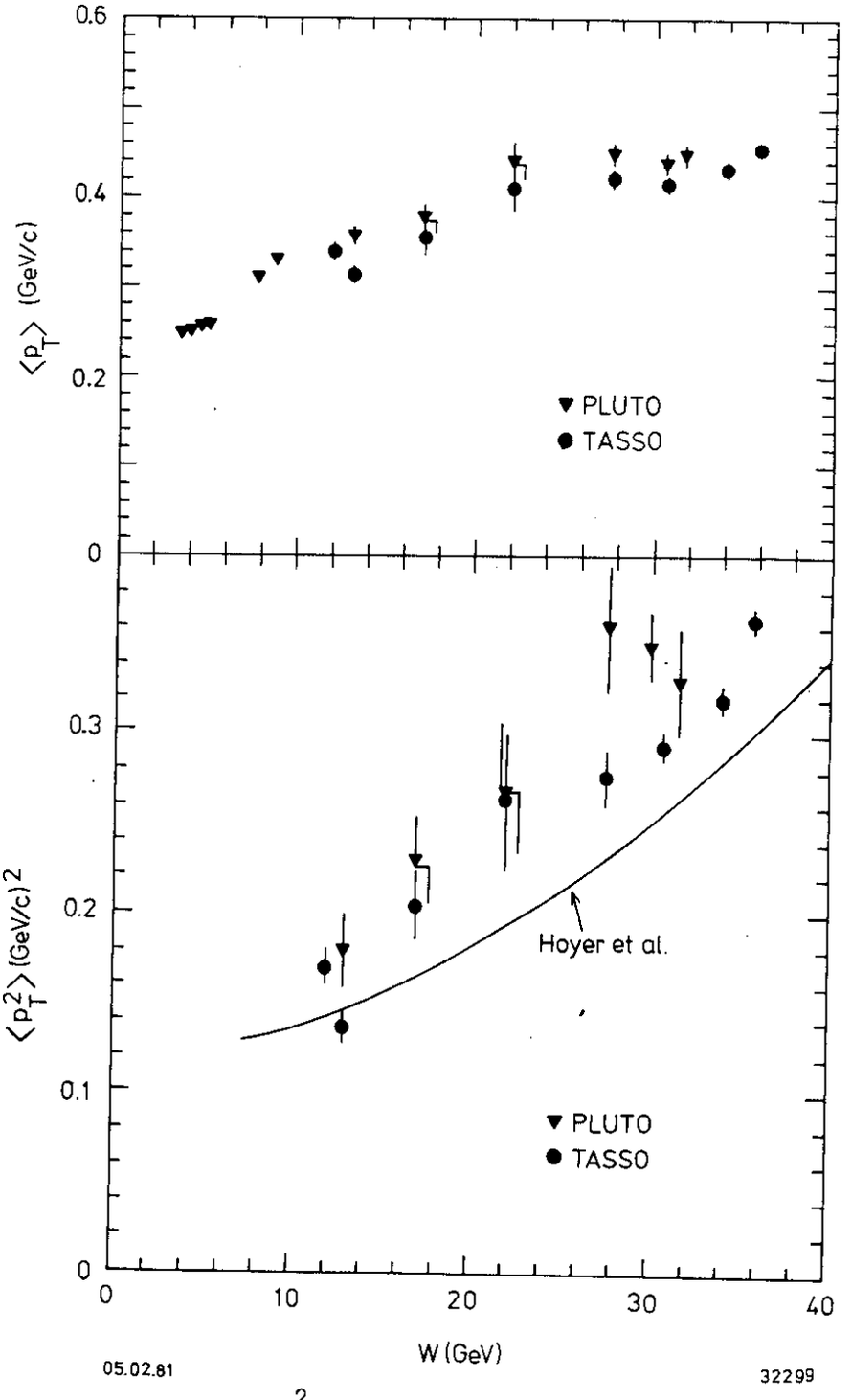

Fig. 3.13 Average P_T and P_T^2 values as a function of the c.m. energy measured by the PLUTO group (Berger et al. 1979b) and TASSO group (Brandelik et al. 1981b). The curve shows a QCD model prediction by Hoyer et al. (1979).

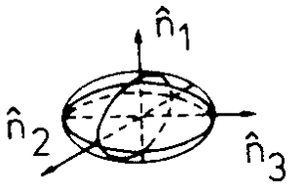

Fig. 3.16 The momentum tensor ellipsoid.

The principal axis is the $\hat{n}_3$ direction which is identical to the sphericity axis. The event plane is spanned by $\hat{n}_2$ and $\hat{n}_3$; $\hat{n}_1$ is normal to this plane and defines the direction in which the sum of the momentum components is minimal.
The normalized eigenvalues

$$Q_i = \frac{\Lambda_i}{\sum p_j^2} = \frac{\sum(\vec{p}_j \cdot \hat{n}_i)^2}{\sum p_j^2} \qquad (3.31)$$

measure the flatness (Q_1), width (Q_2), and length (Q_3) of an event; they satisfy the relation $Q_1 + Q_2 + Q_3 = 1$. The events can therefore be characterized by two of these variables, or e.g. by aplanarity A and sphericity S:

$$A = \frac{3}{2} Q_1, \qquad S = \frac{3}{2}(Q_1 + Q_2) = \frac{3}{2}(1 - Q_3) \qquad (3.32)$$

c) Planar events

In Fig. 3.17 the distribution of

$$\langle p_{Tout}^2 \rangle = \frac{1}{N} \sum_j (\vec{p}_j \cdot \hat{n}_1)^2 = Q_1 \langle p^2 \rangle \qquad (3.33)$$

(= square of momentum component normal to the event plane averaged over the particles in one event) is compared with that of

$$\langle p_{Tin}^2 \rangle = \frac{1}{N} \sum_j (\vec{p}_j \cdot \hat{n}_2)^2 = Q_2 \langle p^2 \rangle \qquad (3.34)$$

(= square of momentum component in the event plane and perpendicular to the jet axis). The data show little increase in $\langle p_{Tout}^2 \rangle$ from low (W = 12 GeV) to high energy (W = 30 to 36 GeV). The distribution of $\langle p_{Tin}^2 \rangle$, however, becomes much wider at high energies; there is a

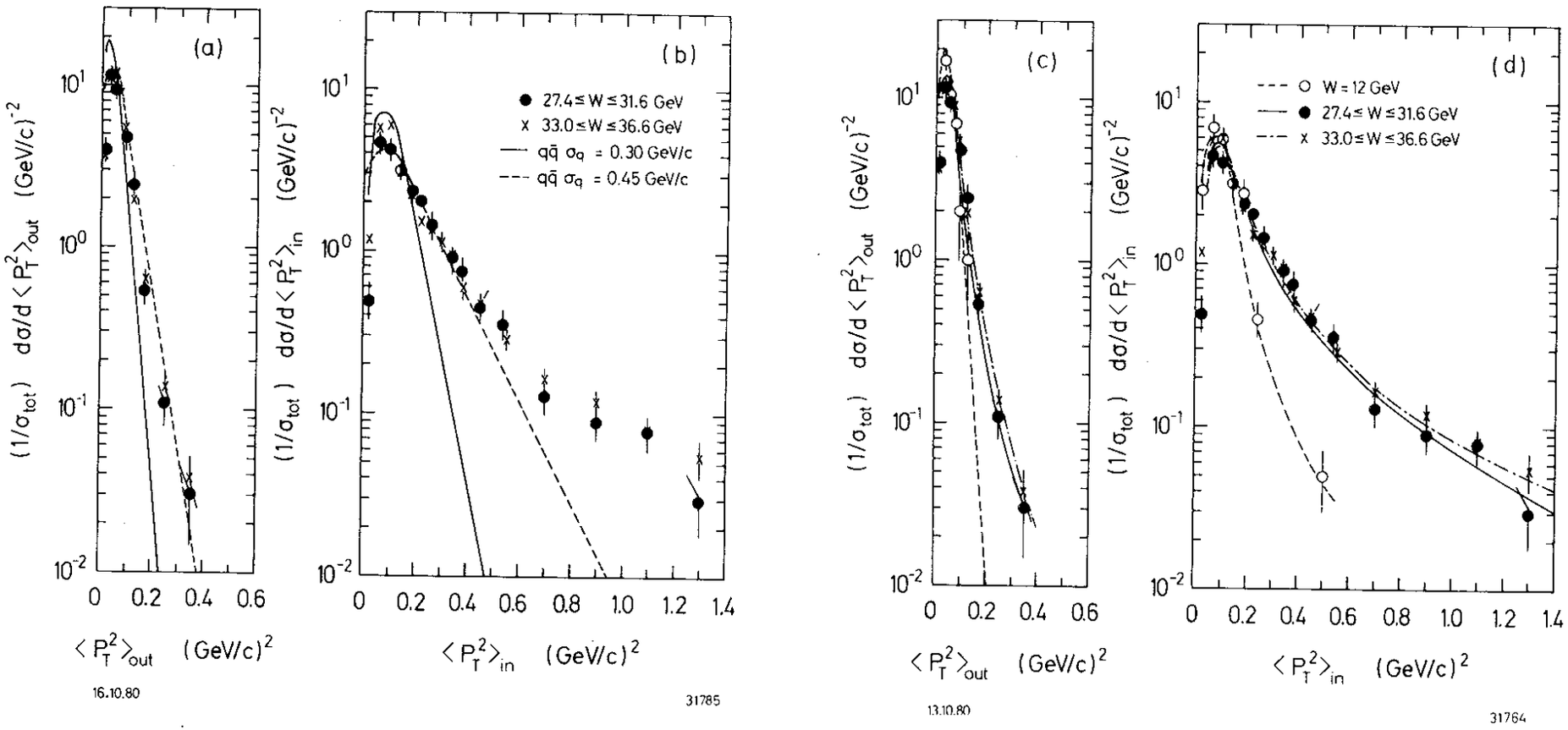

Fig. 3.17 Distributions of the mean transverse momentum squared per event for charged particles, normal to ($\langle P^2_{Tout}\rangle$) and in the ($\langle P^2_{Tin}\rangle$) event plane as measured by the TASSO group (Brandelik et al. 1979b, 1981b) at c.m. energies of 12, 27.4 - 31.6 and 33 - 36.6 GeV.

(a),(b) The curves are the predictions for a $q\bar{q}$ final state with σ_q = 0.3 GeV/c and 0.45 GeV/c, respectively.

(c),(d) The curves show the QCD predictions for α_s = 0.17.

long tail of events with high $\langle P^2_{Tin} \rangle$.

Hadrons resulting from pure $q\bar{q}$ jets will on the average be distributed uniformly around the jet axis. However, some asymmetry between $\langle P^2_{Tout} \rangle$ and $\langle P^2_{Tin} \rangle$ is caused by the bias introduced in choosing the axes. Good agreement with the $q\bar{q}$ model using $\sigma_q = 0.3$ GeV/c is found at low c.m. energy for both distributions. At high energy, the $q\bar{q}$ model with $\sigma_q = 0.3$ GeV/c gives an approximate desription of the $\langle P^2_{Tout} \rangle$ data but fails completely to reproduce the long tail of the $\langle P^2_{Tin} \rangle$ distribution. This discrepancy cannot be cured by increasing σ_q to 0.45 GeV/c (see dashed curve in Fig. 3.17b). One finds that the data contain a certain number of planar events, i.e. events with $\langle P^2_{Tin} \rangle$ much larger than $\langle P^2_{Tout} \rangle$ that cannot be accounted for by the $q\bar{q}$ model independently of the value of σ_q (Brandelik et al. 1979b, Berger et al. 1979b, Bartel et al. 1980).

The same conclusion was reached from a study of the energy flow around the jet axis (Barber et a. 1979b). In this study, individual particle momenta are not reconstructed. Rather, the energy deposited by charged and neutral particles in a calorimeter is determined. The coordinate system is defined by the thrust axis ($\hat{e}_1$ = jet axis),

$$\text{Thrust} = \text{Max} \; \frac{\sum_i |\vec{p}_i \hat{e}_1|}{\sum_i p_i} \tag{3.35}$$

where P_i is the energy deposited in the counter element i; the 'major axis' ($\hat{e}_2$) is perpendicular to $\hat{e}_1$ and is the direction along which the projected energy flow in the plane perpendicular to $\hat{e}_1$ is a maximum:

$$\text{Major} = \text{Max} \; \frac{\sum_i |\vec{p}_i \hat{e}_2|}{\sum_i p_i} \; ; \tag{3.36}$$

and the 'minor axis' which is orthogonal to $\hat{e}_1$ and $\hat{e}_2$. The difference O = Major-Minor is called the oblateness. The distribution of the oblateness is plotted in Fig. 3.18 together with the predictions of the $q\bar{q}$ and a QCD model ($q\bar{q}g$). The 17 GeV data are reproduced by both models. At high energy (27.4 - 31.6 GeV) an excess of events with

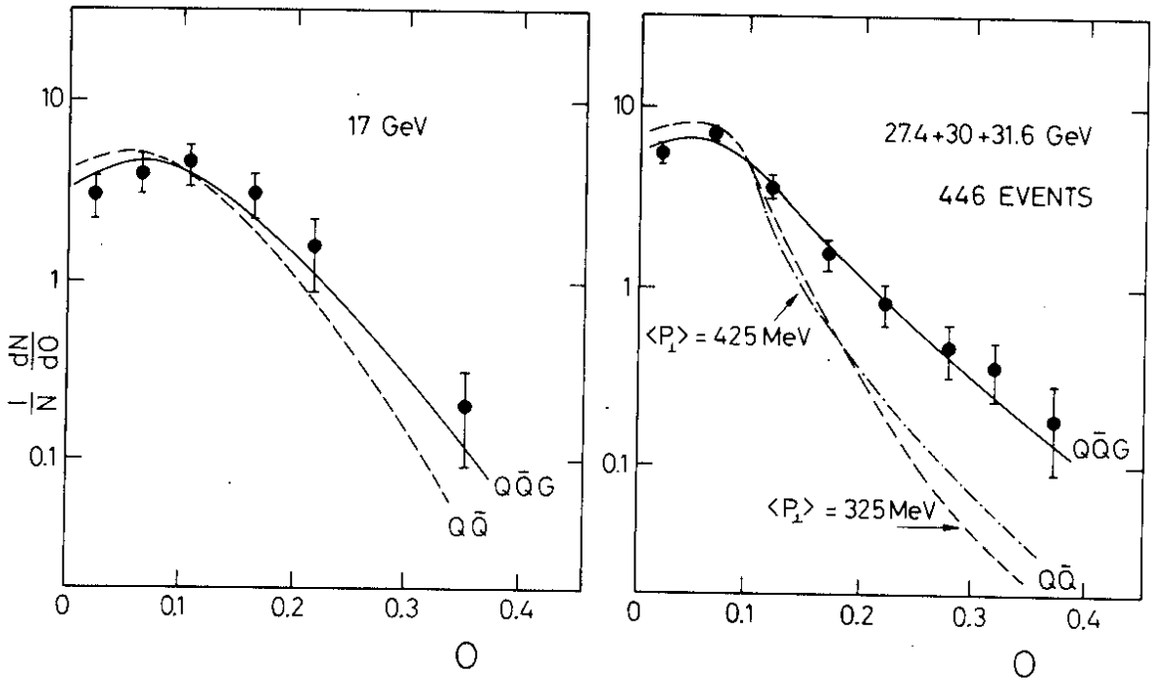

Fig. 3.18 The oblateness distribution, O = Major-Minor, at 17 and 27.4 - 31.6 GeV as measured by the MARKJ group (Barber et al. 1979c). The curves show the predictions for a $q\bar{q}$ model with σ_q = 0.325 GeV/c and 0.425 GeV/c, respectively, and of a QCD model.

large oblateness, i.e. planar events, is observed which is accounted for by the $q\bar{q}g$ model and not by the $q\bar{q}$ model.

A rotation-invariant characterization of the event shape is provided by the Fox-Wolfram (1978, 1979) moments,

$$H_\ell = \frac{4\pi}{2\ell+1} \sum_{m=-\ell}^{\ell} \left| \sum_i \frac{p_i}{W} Y_\ell^m (\Omega_i) \right|^2 = \sum_i \sum_j \frac{P_i P_j}{W^2} P_\ell(\cos\Theta_{ij}) \qquad (3.37)$$

Here Θ_{ij} is the angle between particles i and j. The moments H_ℓ are independent of the particular axes chosen as is evident from the second form in eq.(3.37). Energy-momentum conservation leads to $H_0 = 1$, $H_1 = 0$. For extreme two-jet events $H_2 = 1$. Planar events prefer small H_2 values. In Fig. 3.19 H_2 is shown at 27 GeV (Barber et al. 1980b) together with the predictions for the $q\bar{q}$ (with $\sigma_q = 0.225$ GeV/c) and a QCD model (Ali et al. 1980). Compared to the $q\bar{q}$ model there is an excess of events with low H_2. QCD fits the data well.

d) Three jet structure

The data discussed above demonstrate the existence of planar events. To check whether the particle momenta are distributed uniformly in the plane (disc-like events) or collimated into three jets the TASSO group (Brandelik et al. 1979b, 1980c) followed the procedure of Wu & Zobernig (1979). The events were analyzed in the following way. The particles are grouped into three classes C_1, C_2 and C_3. For each class the 2 x 2 tensor $\sum_j q_{j\alpha} q_{j\beta}$ is diagonalized where $\alpha = 1,2$ correspond to the components in the event plane, and thereby the sphericity axes $\hat{m}_k$ (k = 1,2,3) and the sphericities S_k are determined. By varying the combinations one finds that grouping for which the sum $S_1 + S_2 + S_3$ is minimal. If the event under consideration is indeed a three-jet event, the method reconstructs the three coplanar jet axes $\hat{m}_k$ and associates each particle with one of the three jets. For a two-jet event the method gives degenerate jet axes.

This procedure has been applied at W = 30 GeV to planar noncollinear events selected by requiring $S > 0.25$, $A < 0.08$.

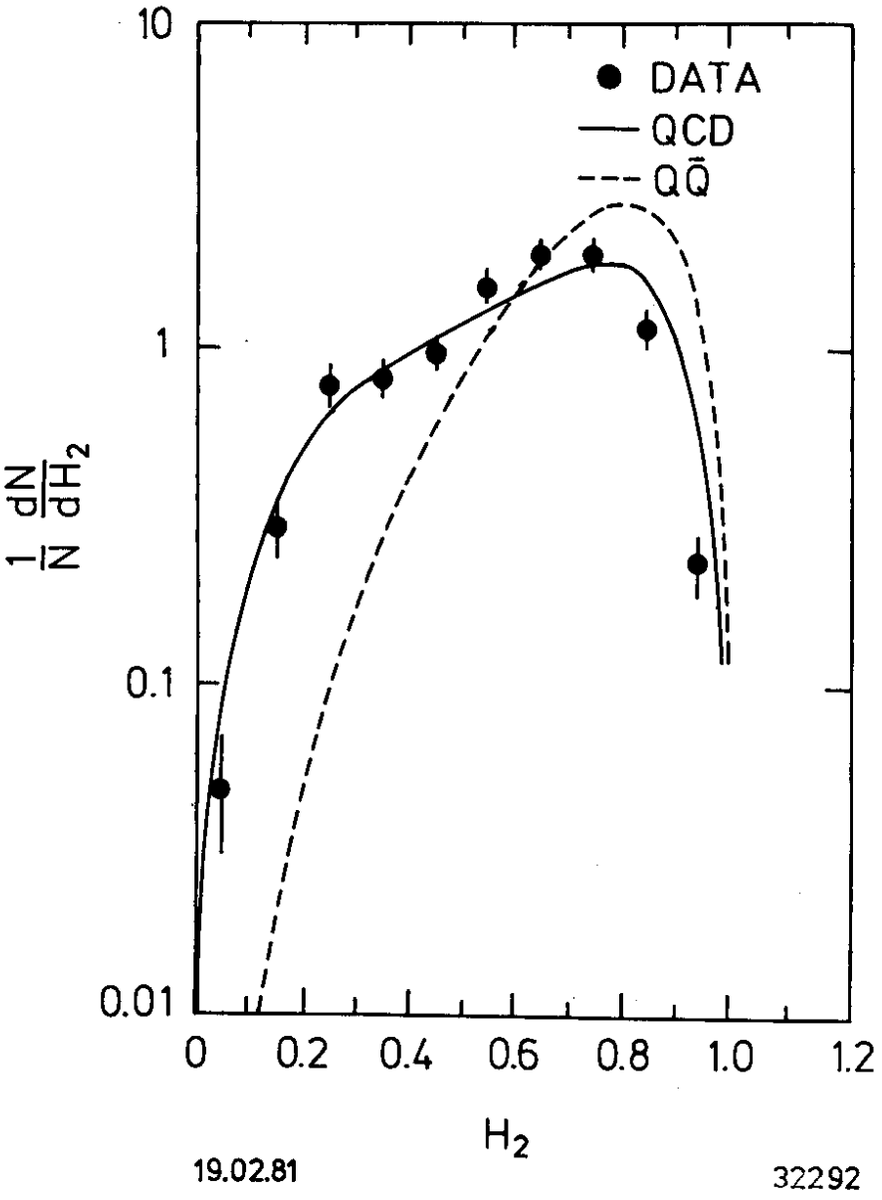

Fig. 3.19 Distribution of the Fox-Wolfram moment H_2 at W = 27 GeV as measured by the Mark J group (Barber et al. 1980b). The curves show the predictons for a $q\bar{q}$ final state and for a QCD model.

Fig. 3.20 shows the distribution of P_T^2 of the charged particles where the P_T of each hadron was calculated with respect to the jet axis it has been associated with. This distribution is compared with the corresponding one for events at 12 GeV analyzed as two jets and, therefore, without cuts in S or A. The P_T^2 behaviour is found to be the same in both cases, i.e. the particles from planar events at high energies are collimated around three coplanar axes in qualitatively the same way as particles from lower energy events are collimated around a single jet axis.

The MARK-J group (Barber et al. 1979b) has searched for a three-jet structure studying the energy flow. Planar events were selected by requiring low thrust, $T < 0.8$, and large oblateness, $O > 0.1$. For each event the Thrust ($= \hat{e}_1$), Major ($= \hat{e}_2$) and Minor ($= \hat{e}_3$) axes were determined. In the event plane spanned by $\hat{e}_1, \hat{e}_2$ the energy was summed in 5^o intervals of the azimuth φ. Fig. 3.21 shows the energy flow averaged over the event sample as a function of φ. The appearance of three maxima is partly a result of the construction of the energy flow diagram and does not in itself prove the existence of three-jet events. Two-jet events or phase space like events also produce three maxima. It is by a quantitative comparison that one can rule out two-jet or phase space like production to be the dominant mechanism. The QCD prediction is in agreement with the data.

The PLUTO group (Berger et al. 1979b) has shown that compared to a $q\bar{q}$ model there is an abundance of low thrust high triplicity events. Low thrust means that these events do not have a two-jet topology. This together with the high triplicity indicates a three-jet structure.

The JADE group (Bartel et al. 1980) has demonstrated the presence of three jet events in a way illustrated in Fig. 3.22.

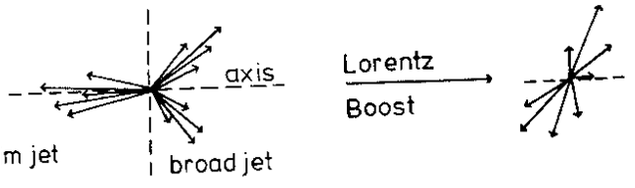

Fig.3.22 Illustration of the procedure used by the JADE group

The broad jet in its own c.m. system

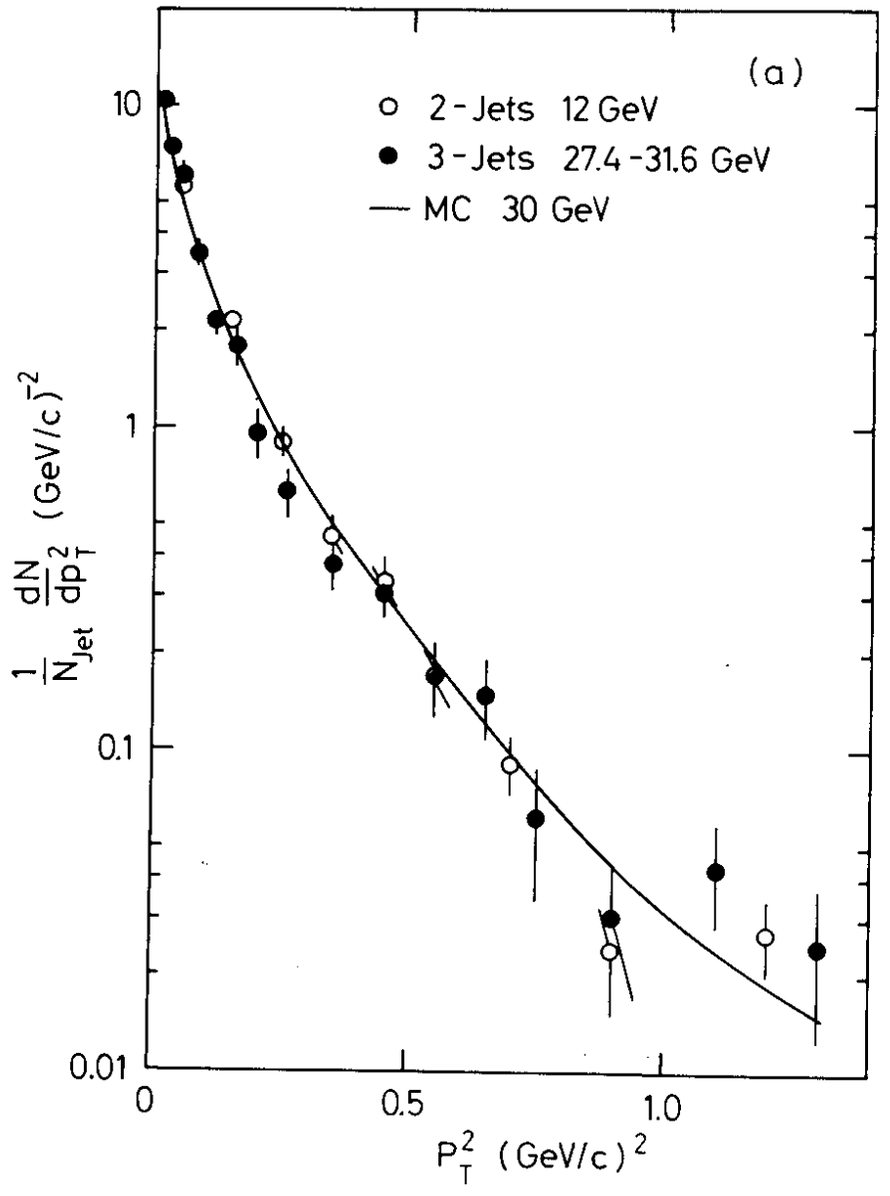

Fig. 3.20 Distribution of the square of the transverse momentum of charged hadrons from planar events with respect to the three axes found by the generalized sphericity method at W = 30 GeV (●). It is compared to the P_T^2 distribution relative to the sphericity axis for all events at W = 12 GeV analyzed as two jet events (o). The curve shows the QCD prediction. The analysis was made by the TASSO group (Brandelik et al. 1980c).

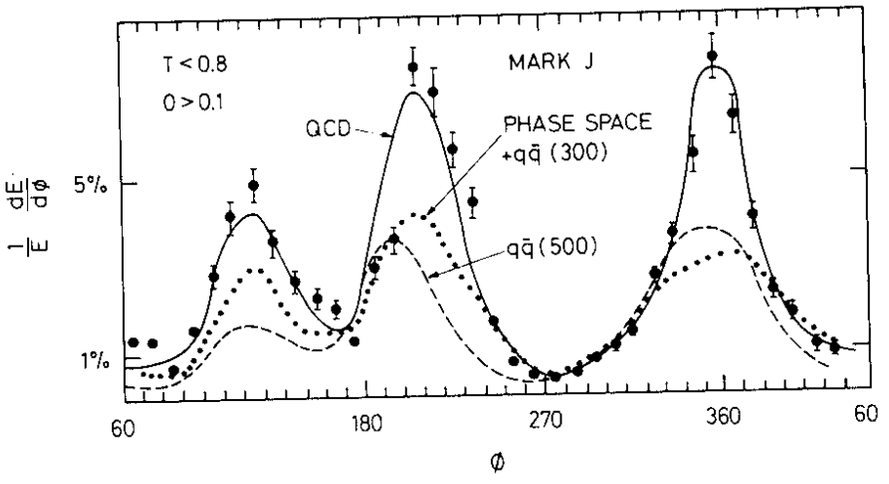

Fig. 3.21 Energy flow for planar events at W = 30 GeV as a function of the azimuth φ as measured by the MARK J group (Barber et al. 1980b). The curves show fits with models for a $q\bar{q}$ final state with σ_q = 0.5 GeV/c, for a mixed phase space and $q\bar{q}$ model and for a QCD model.

For planar events ($Q_2 - Q_1 > 0.1$) produced at W = 30 GeV the thrust axis was determined. For the forward and backward (with respect to the thrust axis) going particles the sum of the transverse momenta, ΣP_{T_i}, was computed separately; the jet with the larger ΣP_T was called the broad jet. A Lorentz transformation into the rest system of the broad jet was made. In this system the thrust T_B of the broad jet was determined. The distribution of T_B is shown in Fig. 3.23 together with the thrust distribution of low energy events (W = 12 GeV) treated as two jets. The two distributions fall on top of each other which leads to the same conclusion drawn before that for high energy planar events the particles are as collimated around three axes as particles are collimated around the common jet axis at lower energies.
Two examples of three-jet events as seen in the JADE and TASSO detectors are displayed in Fig. 3.24.

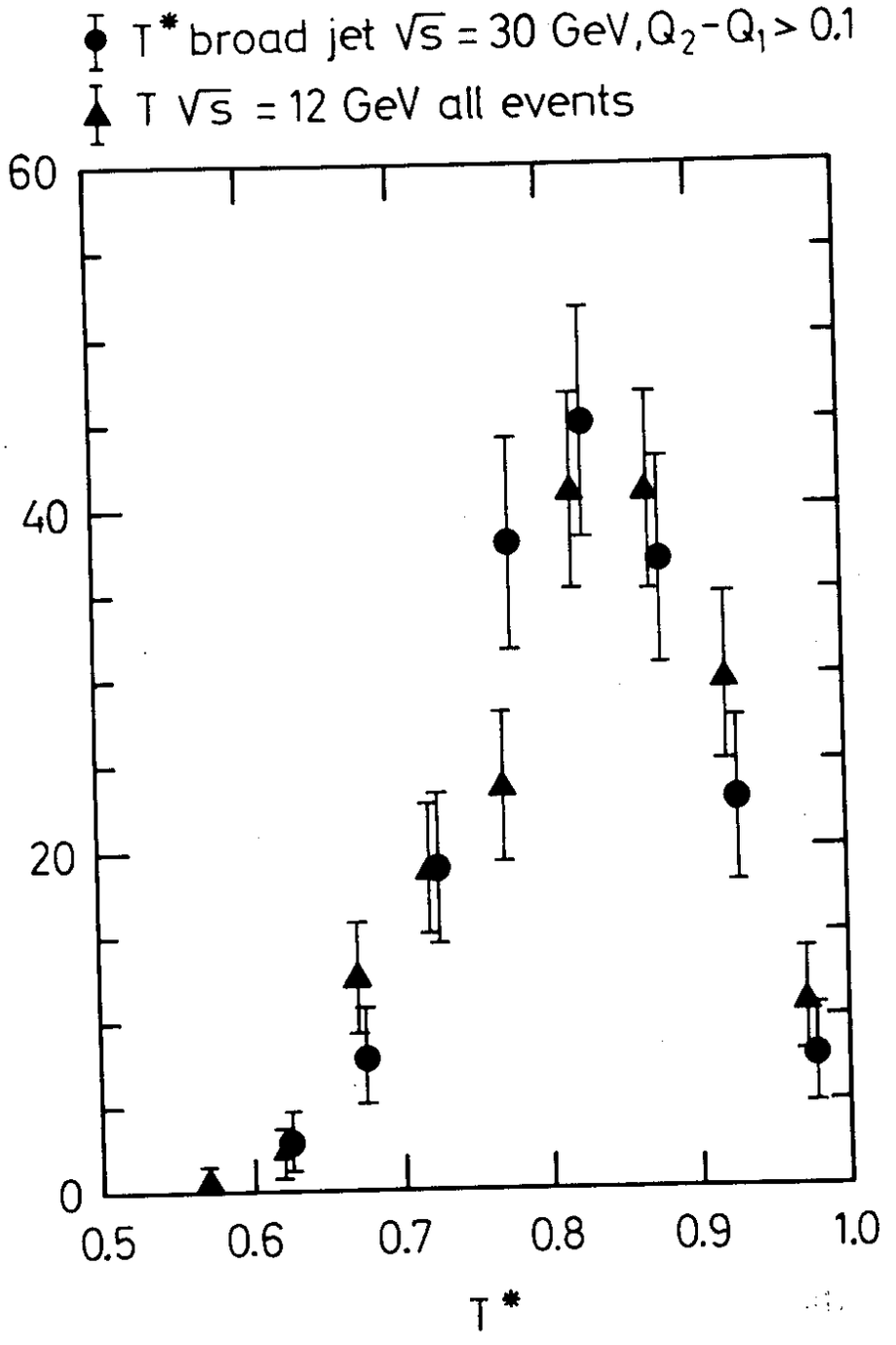

Fig. 3.23 Distribution of thrust for the broad jet of planar events at W = 30 GeV compared with the two jet thrust distribution at W = 12 GeV as measured by the JADE group (Bartel et al. 1980).

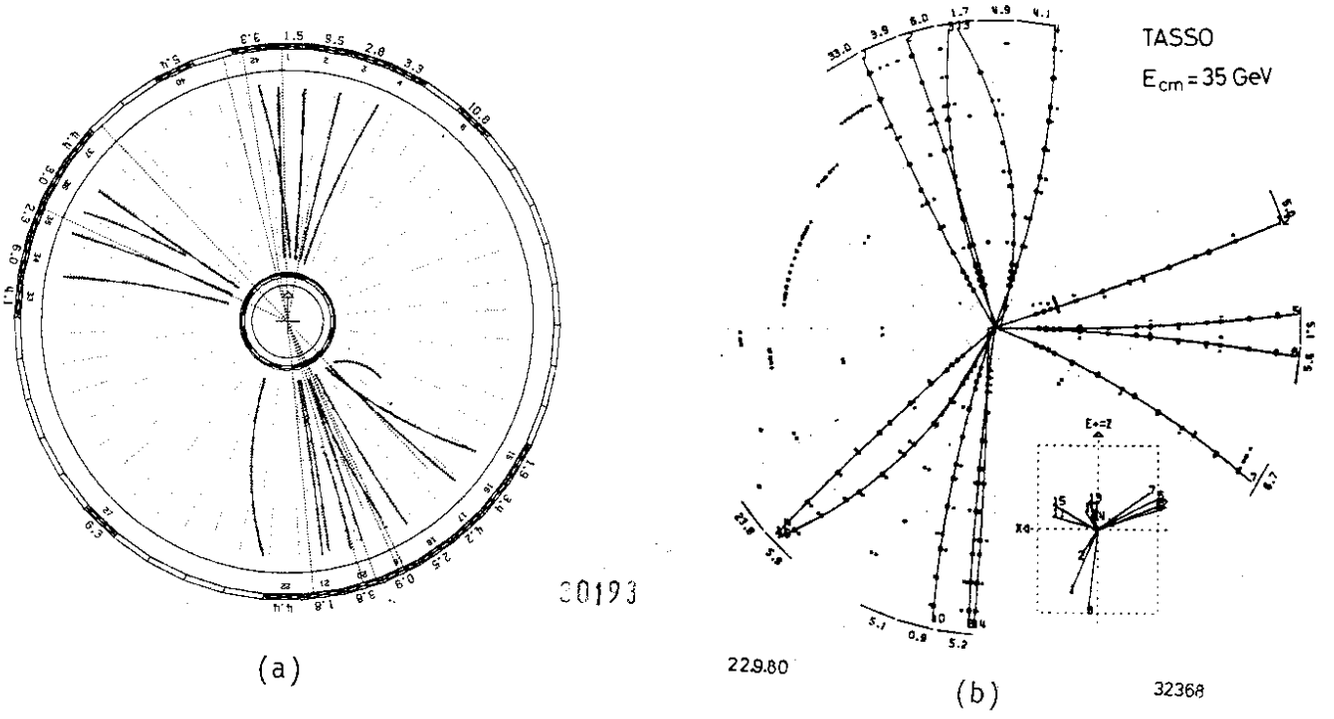

(a) (b)

Fig. 3.24 Examples of three-jet events observed in the JADE and TASSO detectors as viewed along the beam axis. The insert in (b) shows a top view of the event.

e) Quantitative comparison with QCD

The observation of three-jet events in high-energy e^+e^- annihilation qualitatively confirms the prediction of hard gluon bremsstrahlung by leading-order QCD. It does, of course, not rule out other mechanisms as possible sources of these events (see e.g. Preparata & Valenti 1981). Therefore, detailed and quantitative tests are called for. These, however, pose a problem: the hadronization process is not calculable in perturbative QCD. Therefore, for a detailed comparison between experimental results and prediction, the QCD calculations have to be combined with models that describe the quark and gluon fragmentation processes, as discussed already in section 3.2. Only in this way is one able to investigate questions like the overlap between jets, the multijet contribution by semileptonic decays of bottom mesons, the effects of omission of neutrals in some experiments, effects of detector acceptance and resolution, efficiency of the analysis procedures used, and radiative corrections. In the comparison between data and QCD prediction one has then to investigate very carefully to what extent the results are truly independent of the assumptions used in the fragmentation model, and thus can be considered a convincing check of perturbative QCD.[3]

---

3) In the course of such investigations it has been found that a theoretically appealing variable, as e.g. the infrared-stable quantity thrust, is not necessarily the most suitable one for the comparison between measurement and predictions. At present energies many of the particles in the jets have total momenta not much in excess of the average transverse momentum. Monte Carlo simulations show that in this situation a stronger weighting of larger momenta, as in analyses based on the second-rank momentum tensor eqn.(3.29), can lead to more reliable and less model-sensitive results.

Three-jet topology

In the quantitative comparison of the hard-gluon bremsstrahlung predictions with experiment, two elaborate Monte Carlo programs have played a major role, that of Hoyer et al. (1979) and an extension by Ali et al. (1980). Both use the Field-Feynman scheme to describe quark fragmentation (see section 3.2). The first one considers only contributions up to first order in α_s (from diagrams a-c in Fig. 3.25), the second one includes those second order terms that lead to four-jet events (diagrams d-g in Fig. 3.25).

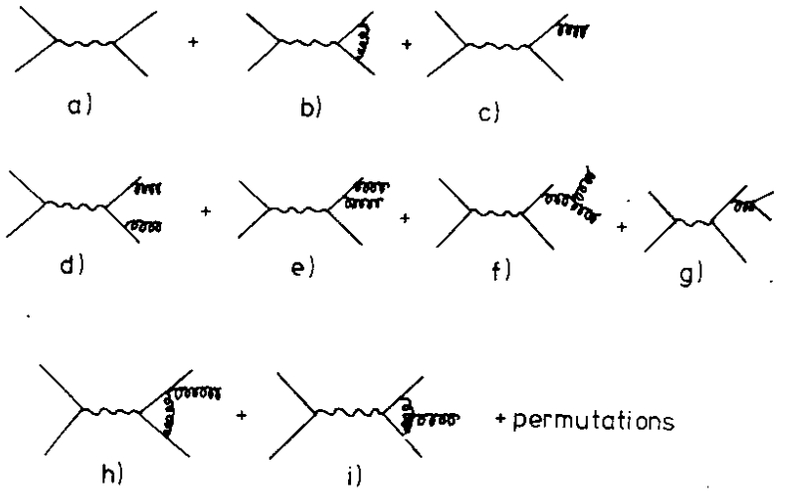

Fig. 3.25 QCD diagram for hadron production

In the analysis of Brandelik et al. (1980c), the strategy followed was to determine first the fragmentation parameters and the unknown strong coupling constant $\alpha_s(Q^2)$ from the data, using as little of the measured information as possible, and then to use the remaining information for a quantitative check which then no longer involves any free parameter. In a first step, from large sphericity events ($S > 0.25$) at $W = 30$ GeV, α_s was determined; no prior assumptions on the fragmentation parameters had to be made at this step, which is not surprising since for large S three-jet production dominates and fragmentation effects play a minor role. In a second step, small sphericity events ($S < 0.25$) were used to determine the fragmentation parameters. It was found that the distributions of $\langle p^2_{Tout} \rangle$, of $x = 2p/W$, and of the charged particle multiplicity n_{CH} at one energy, $W = 30$ GeV, were sufficient to determine these parameters with very little dependence on the input

value of α_s. The resulting values for the fragmentation parameters are quoted in section 3.2. In a third step using these values the events with large sphericity were refitted to obtain the final value for α_s, $\alpha_s = 0.17 \pm 0.02$ (stat.) $\pm$ 0.03 (syst.) for W = 30 GeV. With all free parameters fixed the data were compared to QCD. The energy dependence was tested by comparing with data at 30 GeV and 12 GeV. For 12 GeV, $\alpha_s = 0.21$ was assumed in accord with eq.(1.1). Fig. 3.26 shows the distributions of sphericity, aplanarity ($A = (3/2)Q_1$) and the inclusive x spectrum. Since no 12 GeV information was used in the fits, the agreement between data and theory shows in a parameter-free way that the analysis did indeed succeed to separate perturbative effects which are strong at 30 GeV and hardly observable at 12 GeV, from the nonperturbative effects. Good agreement is also obtained for the distributions of p_T^2, $\langle p_{Tout}^2 \rangle$, and $\langle p_{Tin}^2 \rangle$ (see curves in Figs.3.12, 3.17).

In further tests the specific properties of the high sphericity, planar events ($S > 0.25$, $A < 0.08$), analyzed as three-jet events, were considered. Since only global event-shape parameters described by the momentum tensor but no detailed information on the three-jet structure had been used in determining the fragmentation parameters and the value of α_s, all the three-jet comparisons were parameter-free. A first example is the distribution of p_T^2 for each particle measured with respect to the appropriate jet axis (Fig. 3.20). As another example, Fig. 3.27 shows the distribution of the smallest (Θ_{min}) and the largest angle (Θ_{max}) between any of the three jets. The distribution of Θ_{max} shows the transition from two-jet events (Θ_{max} near 180^0) to large angle gluon bremsstrahlung events. The minimum angle Θ_{min} prefers small values for two-jet events, and larger ones for three-jet events.

The angular correlation between $q,\bar{q}$ and gluon depends on the spin of the gluon. For vector gluons the first order cross section in terms of the scaled parton energies $x_i = 2E_i/W$ is given in eq.(3.26). From this the distribution of the angles Θ_i between the partons can be calculated with the relation eq.(3.14).

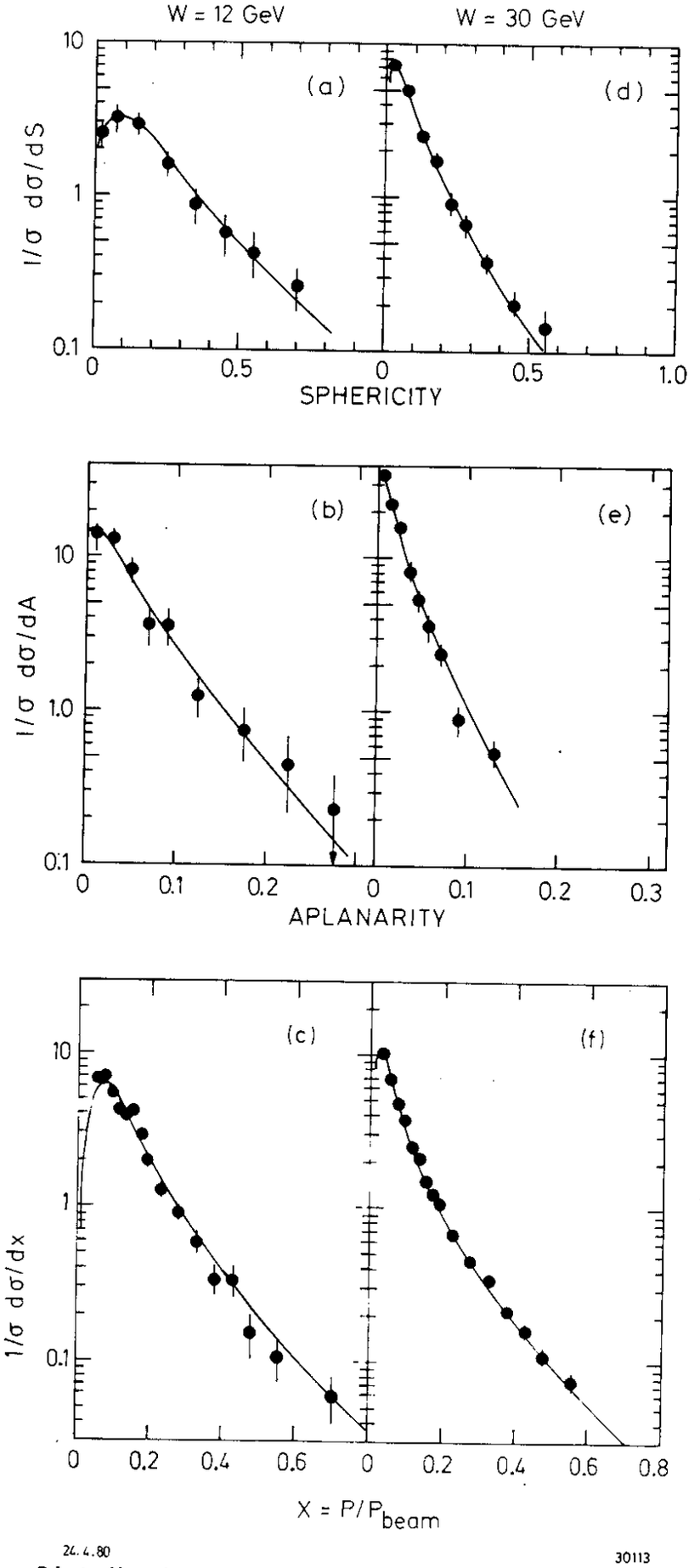

24.4.80 30113

Fig. 3.26 Distributions of the sphericity, aplanarity A = 3/2 Q_1 and the fractional momentum x = 2p/W of charged particles at W = 12 and 30 GeV. The curves at W = 30 GeV show the result of the QCD model fit. The curves at W = 12 GeV are QCD predictions computed from this fit. From the TASSO group (Brandelik et al. 1980c).

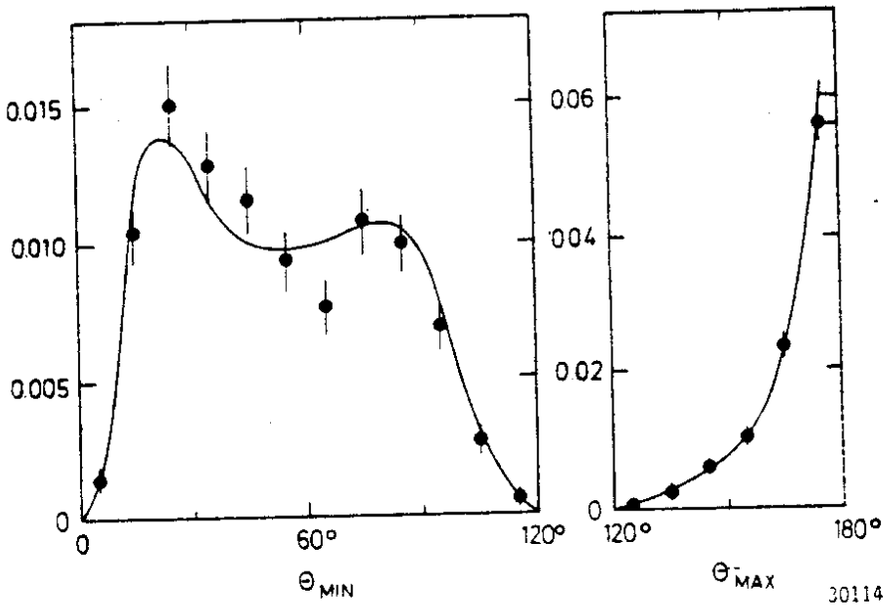

Fig. 3.27 Distribution of the smallest (Θ_{min}) and largest (Θ_{max}) angle between any of the three jets when all events (no S or A cuts) at W = 30 GeV are analysed as three-jet events. The curves show the result of the QCD model. From the TASSO group (Brandelik et al. 1980c).

In order to see that the angular correlation between the jet axes is indeed sensitive to the gluon spin we consider a theory with scalar gluons which leads to (Ellis et al. 1976)

$$\frac{d\sigma}{dx_1 dx_2} = \frac{\tilde{\alpha}_s}{3\pi}\,\sigma_o\,\frac{x_3^2}{(1-x_1)(1-x_2)} \qquad (3.38)$$

where x_3 is the scaled gluon energy and $\tilde{\alpha}_s$ is the gluon quark coupling for the scalar case. The vector expression eq.(3.26) has both collinear and infrared divergencies, whereas for the scalar case there is only a collinear divergence which leads to a somewhat weaker dependence on x_i. Unfortunately, the difference between the scalar and the vector distributions is largest for parton thrust x_1 (or x_2) near 1 where one approaches the two jet configuration, and where smearing effects due to quark and gluon fragmentation are important.

In the analysis of Brandelik et al. (1980d) the angles Θ_i were reconstructed from the charged particle vectors. From the angles the parton energies were determined and ordered such that $x_1 \geq x_2 \geq x_3$. Since quarks and gluon are not identified one has to include in eqs.(3.26) and (3.38) the cyclic permutations of x_1, x_2 and x_3.

In order to avoid the problematic area near $x = 1$ only events with $x \leq 0.9$ were considered. The distribution most sensitive to the discrimination between vector and scalar gluons was found to be the distribution of the angle $\tilde{\Theta}$ illustrated in Fig. 3.28 (Ellis & Karliner 1979). The $q\bar{q}g$ system is Lorentz boosted into the c.m. frame of partons 2 and 3 (one of which by virtue of the ordering of the x_i is more likely to be the gluon) and $\tilde{\Theta}$ measures the angle between the 2, 3 axis and the parton 1. Assuming massless partons

$$\cos\tilde{\Theta} = \frac{x_2 - x_3}{x_1} = \frac{\sin\Theta_2 - \sin\Theta_3}{\sin\Theta_1}$$

Fig. 3.29 compares the observed $\cos\tilde{\Theta}$ distribution with the Monte Carlo predictions for vector and scalar gluons, where the Monte Carlo events were analyzed in the same way as the measured

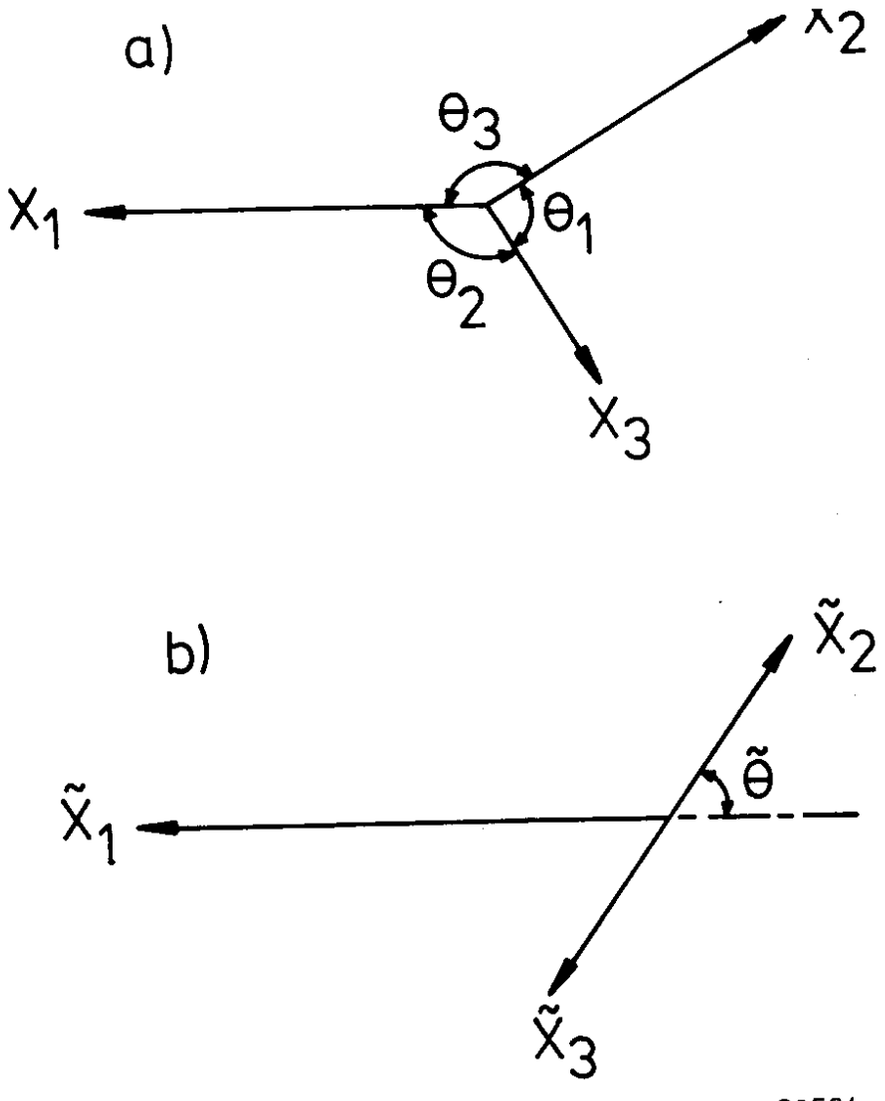

29.8.80 30524

Fig. 3.28(a) Momenta and angles of a $q\bar{q}g$ final state in the c.m. frame.

(b) The $q\bar{q}g$ final state transformed to the rest frame of particles 2 and 3.

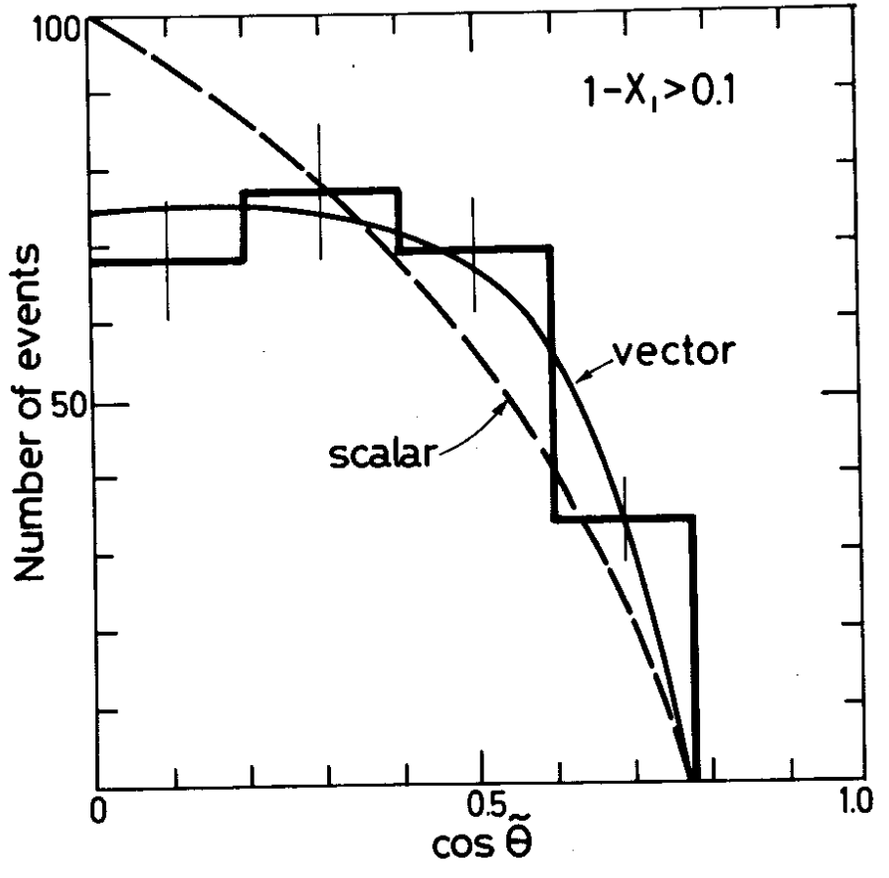

01.09.80 30544

Fig. 3.29 Observed distribution of cosΘ for events with lower parton thrust $1-x_1 > 0.1$ at W = 27.4 - 36.6 GeV. The solid line shows the QCD prediction, the dotted line shows the prediction for scalar gluons. From the TASSO group (Brandelik et al. 1980d).

data.[4] Spin 1 is clearly preferred over spin 0, the latter being disfavoured by 4 standard deviations.

A promising attempt to reconstruct the original parton distributions from the measured data has been made by Berger et al. (1980c). The events have been classified as 2-, 3-, 4-jet events according to the number of particle clusters observed (Daum et al. 1980). Fig. 3.30 shows the resulting parton thrust distribution for 3-jet events. Note that in $x_1 \lesssim 0.9$ this distribution is a factor of 3-5 below the thrust distribution for all events determined using eqn.(3.19). The QCD prediction (curve) agrees with the data while a scalar gluon theory would not describe the data well.

The value of α_s

The number of three-jet events is directly related to the value of the 3 quark gluon coupling strength, α_s. The α_s values obtained at energies of 30 - 35 GeV are summarized in Table 3. The result of the MARK-J group (Barber et al. 1979c, Newman 1980) was obtained from the oblateness distribution of the broad jet. The procedure used by the TASSO group (Brandelik et al. 1980c) has been described above. A similar procedure was used by the JADE group (Yamada 1980). The PLUTO group (Berger et al. 1980c) has determined α_s with the help of the cluster method comparing the observed number of three-jet events with those predicted by QCD.

---

4) For a fixed x_1, $W(\cos\tilde{\Theta})$ is of the form $1 + a(x_1)\cos\tilde{\Theta}$, $a(x_1) > 0$. Due to the ordering $x_1 \geq x_2 \geq x_3$, $\cos\tilde{\Theta}$ can vary between 0 and 1 only for $x_1 = 1$. As x_1 decreases the maximum value of $\cos\tilde{\Theta}$ decreases too; e.g. for $x_1 = 0.9$, $\mathrm{Max}(\cos\tilde{\Theta}) = 0.78$ and for the symmetry point $x_1 = x_2 = x_3 = 0.67$, $\cos\tilde{\Theta}$ is limited to the single value $\cos\tilde{\Theta} = 0$. Integration over x_1 therefore leads to a distribution that is heavily weighted towards small $\cos\tilde{\Theta}$ values.

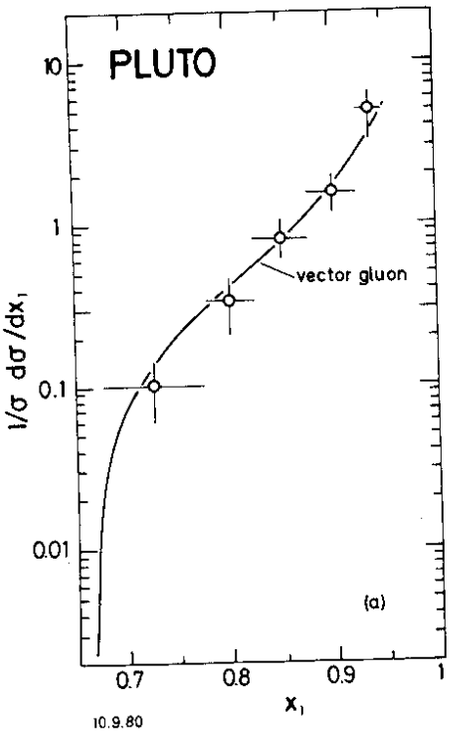

Fig. 3.30 Distribution of the parton thrust x_1 at W = 30 GeV as determined from a cluster method by the PLUTO group (Berger et al. 1980c). The curve shows the prediction of a QCD model.

All four experiments are seen to agree on the value of α_s, yielding an average of $\alpha_s = 0.17 \pm 0.01$ with a systematic uncertainty of 0.03. We add a few remarks. Although the value of α_s was found independently of the fragmentation parameters, the analyses were based on a particular way of describing the hadronization process, namely the Field-Feynman model. The inclusion of second order corrections seems to have a small effect on α_s. This may be seen from the results of Brandelik et al. (1980c):

$\alpha_s = 0.19 \pm 0.02$ with first order terms
$= 0.17 \pm 0.02$ including also second order terms.

However, the $O(\alpha_s^2)$ calculation does not include all diagrams; e.g. diagrams h,i of Fig. 3.25 are missing. An evaluation of all second order terms has recently been made by three groups, R.K. Ellis et al. (1980), Fabricius et al. (1980), and Vermaseren et al. (1980). Although working all in the $\overline{MS}$ scheme they arrive at conflicting results which lead to different conclusions. Fabricius et al. find that the $O(\alpha_s^2)$ contributions are comparatively small, amounting to ≈30 % of the first order result for thrust T = 0.95 and decreasing for smaller T values except in the region where four jets contribute. The two other groups find the second order contribution to three-jet production to be of the same size as the first order one. However, the energy partition between the jets and therefore the distributions of the angles between the jets is almost the same in $O(\alpha_s^2)$ as in $O(\alpha_s)$. This is not surprising since the divergence problems in $O(\alpha_s^2)$ arise when one gluon is hard and the other is soft (see diagram 3.31a) which is counteracted by the vertex corrected diagram 3.31b).

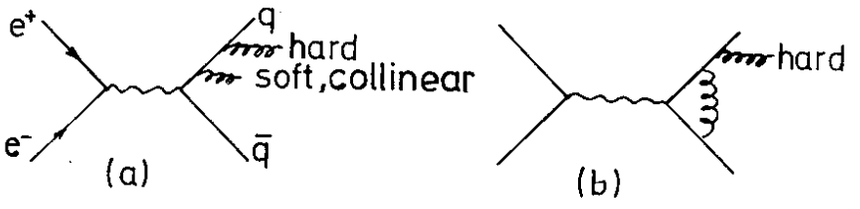

Fig. 3.31 Examples of higher order QCD diagrams

Kinematically both diagrams correspond to the first order diagrams. The question of convergence of perturbative QCD in three-jet production

is obviously of prime importance and deserves a special effort by theorists.

f) Soft gluon emission

The previous section primarily dealt with the emission of a single hard gluon. The multiple emission of soft or collinear gluons contains infrared divergences and many - in fact infinitely many - diagrams become important and have to be summed. No rigorous theory does yet exist but a first step towards understanding these processes has been made (Dokshitzer et al. 1978, 1980, Basham et al. 1978, 1979, Konishi et al. 1979, Curci et al. 1979, Fox & Wolfram 1979, Kajantie & Pietarinen 1980, Parisi & Petronzio 1979, Lo & Sullivan 1979, Azimov et al. 1980, Rakow & Webber 1979, Halzen & Scott 1980, Marquardt & Steiner 1980, S.D.Ellis & Stirling 1980, Baier & Fey 1981). Consider again gluon bremsstrahlung, $e^+e^- \to q\bar{q}g$. The first order differential cross section diverges like $1/\Theta$ as the angle Θ between the q and the $\bar{q}$ direction goes to zero (Fig.3.32a).

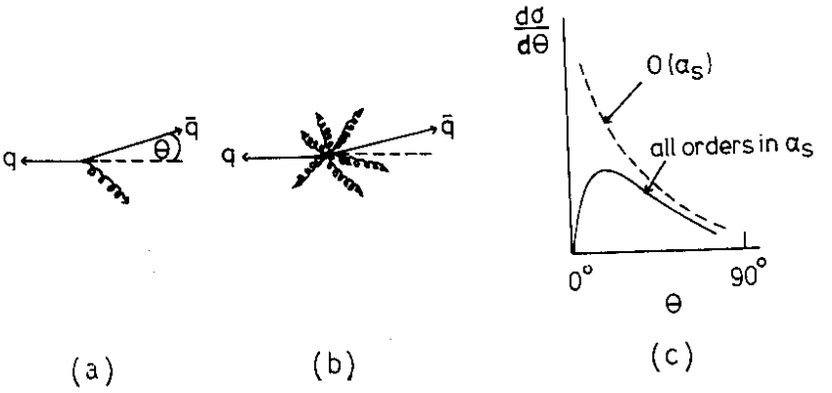

Fig. 3.32 Illustration for soft-gluon emission.

The divergence is cancelled by the sum of multigluon emissions (Fig. 3.32b). Summing the leading logarithmic terms to all orders of perturbation theory, one finds that the cross section approaches zero as $\Theta \to 0$; the original quark and antiquark are always slightly deflected by the multiple emission of gluons.

Dokshitzer et al. (1978) proposed to relate the parton angular distribution to the energy weighted two particle differential cross section,

$$\frac{d\Sigma}{d\cos\Theta} = \sum_{a,b} \int dx_a \, dx_b \, x_a \, x_b \, \frac{d\sigma}{dx_a dx_b d\cos\Theta}$$

where a,b are any two particles emitted in the event with fractional momenta $x_a, x_b, (x = P/E_{beam})$ and angle $(\pi-\Theta)$ between them, and the summation is performed over all two-particle combinations. This energy-energy correlation has been studied by Berger et al. (1980d) between 7.7 and 31.6 GeV. In contrast to earlier hopes (Berger et al. 1980e) the data are not able to distinguish between jet fragmentation and multiple soft gluon radiation effects. As shown by Fig. 3.33 the data can be described by a variety of models, by two jet production ($q\bar{q}$), by hard gluon bremsstrahlung ($q\bar{q}g$) - both including fragmentation, and by a leading log calculation summing over all soft gluons.

It is clear that at presently available energies the angular region in which the damping effect due to multiple soft gluon radiation is expected, is still within the region dominated by quark fragmentation effects. This also makes it difficult to assess quantitatively the effect of soft gluon emission on the transverse momentum distribution in $q\bar{q}$ two-jet events studied by Berger et al. (1980f).

g) Quark and gluon fragmentation

Three-jet events interpreted as hard-gluon bremsstrahlung offer the possibility to compare directly quark and gluon fragmentation. It is generally expected that gluon jets will yield a higher multiplicity and a softer hadron spectrum as well as a larger jet cone angle than quark jets of the same characteristic momentum (see e.g. Konishi et al. 1979). The reason is the larger colour charge of gluons which leads to a larger parton multiplicity in their evolution.

In gluon bremsstrahlung ($e^+e^- \rightarrow q\bar{q}g$) the gluon has on average, a lower energy than quark or antiquark. However, in practice the identification of the gluon amongst the three jets sofar has been possible on a statistical basis only. An attempt to compare gluon and quark fragmentation has been presented by the JADE group (Petersen 1980, Yamada 1980, Bartel et al. 1981). In planar events, defined by $Q_2 - Q_1 > 0.07$, the slim jet (q) and the two subjets which together form the broad jet were identified (see Fig. 3.22). The subjet with

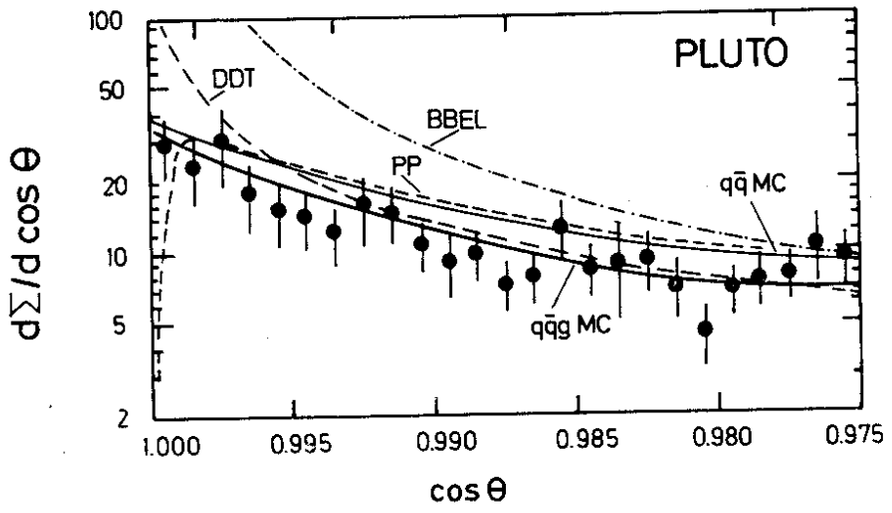

Fig. 3.33 Opposite side energy weighted two particle differential cross section at W = 30 GeV. The curves show predictions for a $q\bar{q}$ final state with hadronization ($q\bar{q}$MC), hard-gluon bremsstrahlung with fragmentation BBEL (Basham et al. 1978, 1979), $q\bar{q}g$MC (Hoyer et al. 1979), and for QCD models summing leading logs DDT (Dokshitzer et al. 1980), PP (Parisi & Petronzio 1979). From the PLUTO group (Berger et al. 1980d).

the smaller angle relative to the slim jet was called the "gluon jet" (g), the other the "quark jet" ($\bar{q}$). Monte Carlo studies indicated that in 50 % of the events the gluon jet is correctly identified. The particle yield is plotted in Fig. 3.34 as a function of the fractional angle Θ/Θ_{max} between the particle and the q direction (a) for the region between q and $\bar{q}$ and (b) between q and g. One finds that in the center region, $\Theta/\Theta_{max} \approx 0.5$, the particle angular density in the region between q and g is considerably larger than between q and $\bar{q}$. It is unclear whether this difference is due to higher order effects in QCD or whether it indicates a difference between quark and gluon fragmentation. The string model approach to $q\bar{q}g$ has predicted such a difference (Andersson et al. 1980).

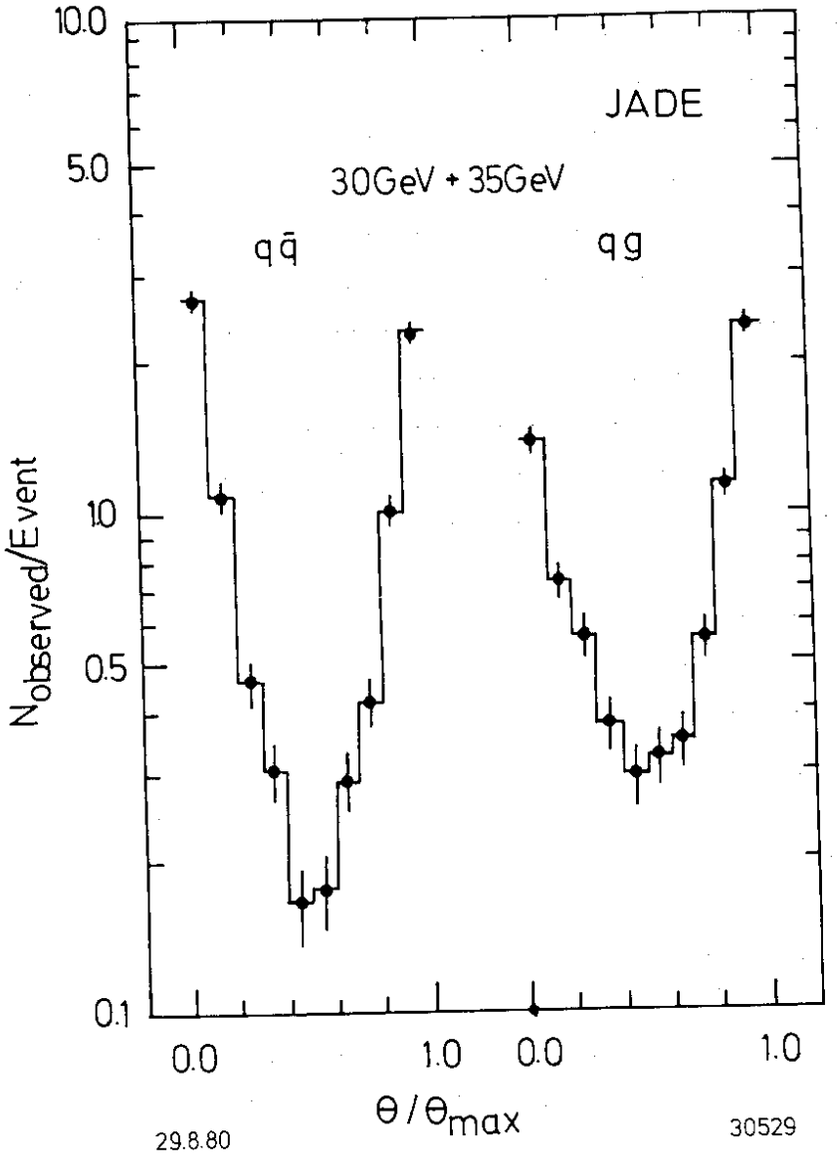

Fig. 3.34 Angular distribution Θ/Θ_{max} of particles in the $q\bar{q}$ and qg regions (defined in the text) as measured by the JADE group at W = 30 - 35 GeV (Yamada 1980).

4. SUMMARY AND CONCLUSIONS

QCD, the candidate theory of the strong interactions, has been remarkably successful in the past years. Several of its outstanding predictions were confirmed by experiment. The first striking success was the experimental corroboration of the pattern for scaling violations in nucleon structure functions predicted by QCD. In its ability to describe the Q^2 evolution of the structure functions QCD has proved superior to all other known field theories. The quantitative evaluation of the observed scaling violations and the determination of α_s or Λ has been somewhat hampered by the smallness of the available Q^2 range and the fact that the perturbative effects are small and depend only logarithmically on Q^2. The inclusion of low-Q^2 data which increases the lever arm in Q^2 makes the analysis sensitive to nonperturbative effects. The presence of such effects is indicated by the fact that the value of Λ obtained from the experiments has shown a tendency to decrease as the experiments reached higher Q^2. Values of α_s obtained from inelastic lepton nucleon scattering lie in the range $0.15 \lesssim \alpha_s \lesssim 0.3$ for an effective Q^2 of the order of 50 GeV^2.

A particularly clean test of QCD would be possible by a precision measurement of the total cross section for e^+e^- annihilation into hadrons. Unfortunately the QCD correction to the quark parton value of $R = \sigma_{tot}(e^+e^-)/\sigma_{\mu\mu}$ is of the same size as the systematic uncertainties in the present experimental values of R. Magnitude and energy dependence of the measured R are consistent with QCD for a value of $\alpha_s = 0.24 \pm 0.26$ at $Q^2 = W^2 \sim 1000$ GeV^2.

In the quarkonium process $e^+e^- \to T \to$ hadrons, the topology of the direct T decays is found to put stringent limits on any gluonic type of theory. The data from DORIS experiments exclude colourless gluons and are inconsistent with decay into three scalar gluons. They agree well with a decay into three vector gluons. The decay width in first order QCD leads to $\alpha_s = 0.17 \pm 0.04$ at the T mass. Higher order corrections are still unknown.

The observation of three-jet events in high energy e^+e^- annihilation into hadrons may be considered a major triumph of the theory. QCD had predicted such events to occur as a result of hard gluon bremsstrahlung. Close examination of the details of the three-jet process at PETRA shows consistency with QCD and confirms the vector nature of the gluon. From the rate of three-jet events the experiments determine $\alpha_s = 0.17 \pm 0.01$ (stat.) $\pm$ 0.03 (syst.) at $Q^2 \approx 1000$ GeV^2; not all second order terms in α_s, however, were included in the analyses.

In conclusion the experimental results show a strong preference for a theory with coloured vector gluons - just what QCD is. Consistent results are found for the value of the quark gluon coupling strength in lowest order from a variety of different processes. With the inclusion of higher orders it may soon be possible to measure the QCD scale parameter Λ; a comparison with lattice QCD predictions will then be very interesting (Creutz 1980, Münster & Weisz 1980, Hasenfratz & Hasenfratz 1980, Kogut et al. 1981). Two important characteristics of QCD have not yet been verified by experiment: Asymptotic freedom, i.e. the decrease towards zero of the strong coupling constant with increasing Q^2, and the existence of the three-gluon vertex. The first point will require higher Q^2 than presently available or a study of "cleaner" processes such as $\gamma\gamma$ scattering at large Q^2. The second aspect may eventually be tested in the decays of heavy quarkonia, in particular of toponium if it is found.

Acknowledgements

We are indebted to J. Gayler, M. Holder, G. Kramer, E. Lohrmann, and T. Walsh for a critical reading of parts of this paper. We thank Mrs. E. Hell for her patience with the manuscript.

Table 1 Ratio of anomalous dimensions from moments of xF_3

d_n/d_m	ABCLOS $Q^2>1$ GeV^2 (Nachtmann moments)	CDHS $Q^2 > 6$ GeV^2 (Nachtmann moments)	CDHS $Q^2 > 6$ GeV^2 (ordinary moments)	QCD in leading order	QCD in next order*	scalar gluons**
d_5/d_3	1.50 ± 0.08	1.34 ± 0.12	1.58 ± 0.12	1.46	1.60	1.12
d_6/d_4	1.29 ± 0.06	1.18 ± 0.09	1.34 ± 0.07	1.29	1.39	1.06

* slope in $\ell nM_n(Q^2)/\ell nM_m(Q^2)$ plot at $Q^2 = 10$ GeV^2, using $\Lambda = 0.4$ GeV independent of the renormalization scheme (Pennington & Ross 1979).

** Bailin & Love (1974)

Table 2 Determination of α_s from the J/ψ and T hadronic and leptonic decay widths using eq.(3.10). The values shown are averages from Boyarski et al.(1975), Bemporad (1975), Burmester et al. (1976), Brandelik et al. (1979a) for the J/ψ and from Albrecht et al. (1980), Niczyporuk et al. (1981a) for the T.

	J/ψ	T
Γ_{tot} (keV)	64 ± 10	$39\ ^{+\ 19}_{-\ 10}$
Γ_{ee} (keV)	4.6 ± 0.4	1.29 ± 0.07 ± 0.14
Γ_{dir} (keV)	38 ± 10	$29\ ^{+\ 20\ +\ 9}_{-\ 11\ -\ 7}$
α_s	0.18 ± 0.01	0.16 ± 0.04

Table 3 Determination of α_s around W = 30 GeV. First error is statistical, second systematic.

JADE	0.18 ± 0.03 ± 0.03*
MARK J	0.19 ± 0.02 ± 0.04*
PLUTO	0.15 ± 0.03 ± 0.02
TASSO	0.17 ± 0.02 ± 0.03

* preliminary value

LITERATURE CITED

Abbot, L. F., Barnett, R. M. 1980. Ann. Phys. 125:276. See also Abbot, L. F., Berger, E. L., Blankenbecler, R., Kane, G. L. 1979. Phys. Lett. 88B:157; Abbot, L. F., Atwood, W. B., Barnett, R. M. 1980. Phys. Rev. D22:582

Albrecht, H. et al. 1980. DESY Report 80/30

Ali, A. et al. 1979. Z. Physik C2:33; Phys. Lett. 83B:375

Ali, A. et al. 1980. Phys. Lett. 93B:155; Nucl. Phys. B168:409

Altarelli, G., Parisi, G. 1977. Nucl. Phys. B126:298

Anderson, H. L. et al. 1977. Phys. Rev. Lett. 38:1450

Andersson, B., Gustafson, G., Sjöstrand, T. 1980. Phys. Lett. 94B:211 and references quoted therein

Appelquist, T., Politzer, H. D. 1975. Phys. Rev. Lett. 34:43; Phys. Rev. D12:1404

Atwood, W. B. et al. 1976. Phys. Lett. 64B:479. See also Atwood, W. B. 1975. Electron Scattering off Hydrogen and Deuterium at 50^{o} and 60^{o}. SLAC Report 185. See also Miller, G. et al. 1972

Aubert, J. J. et al. 1980. XX Int. Conf. on High Energy Physics, Madison, Wisconsin

Azimov, Ya. I., Dokshitzer, Yu. L., Khoze, V. A. 1980. Proc. XV Winter School of Leningrad Inst. Nucl. Phys. 1980, p.3-63

Babcock, J. B., Cutcosky, R. E. 1980. Carnegie-Mellon Univ. Report COO-3066-144

Bace, M. 1978. Phys. Lett. B78:132

Bacci, C. et al. 1979. Phys. Lett. 86B:234

Baier, R., Fey, K. 1981. Nucl. Phys. B179:49

Bailin, D., Love, A. 1974. Nucl. Phys. B75:159

Ball, R. C. et al. 1979. Phys. Rev. Lett. 42:866

Barber, D. P. et al. 1979a. Phys. Rev. Lett. 43:901

Barber, D. P. et al. 1979b. Phys. Rev. Lett. 43:830

Barber, D. P. et al. 1979c. Phys. Lett. 89B:139

Barber, D. P. et al. 1980a. Phys. Rev. Lett. 45:1904

Barber, D. P. et al. 1980b. Physics Reports and MIT Rep. 107

Barbieri, R., Gatto, R., Kögerler, R., Kunszt, Z. 1975. Phys. Lett. 57B:455

Bardeen, W. A., Buras, A. J., Duke, D. W., Muta, T. 1978. Phys. Rev. D18:3998

Bardeen, W. A., Fritzsch, H., Gell-Mann, M. 1973. In Scale and Conformal Symmetry in Hadron Physics (ed. by R. Gatto), New York

Barish, B. C. et al. 1978. Phys. Rev. Lett. 40:1414
Barnett, R. M. 1980. XXth Int. Conf. on High Energy Physics, Madison, Wisconsin and SLAC-PUB-2579
Barnett, R. M., Dine, M., McLerran, L. 1980. Phys. Rev. D22:594
Bartel, W. et al. 1979. Phys. Lett. 88B:171
Bartel, W. et al. 1980. Phys. Lett. 91B:142
Bartel, W. et al. 1981. DESY Report 81-009
Basham, C. L. et al. 1978. Phys. Rev. Lett. 41:1585 and 1979. Phys. Rev. D17:2298; 1979. Phys. Rev. D19:2018
Baulieu, L., Kounnas, C. 1979. Nucl. Phys. B155:429
Bemporad, C. 1975. Proc. 7th Int. Symp. Lepton and Photon Interactions at High Energies, Stanford, p.113
Benvenuti, A. et al. 1979. Phys. Rev. Lett. 42:1317
Berends, F. A., Gaemers, K.J.F., Gastmans R. 1974. Nucl. Phys. B68:541
Berends, F. A., Kleiss, R. 1980. DESY Report 80/66
Berger, Ch. et al. 1978. Phys. Lett. 76B:243
Berger, Ch. et al. 1979a. Phys. Lett. 81B:410
Berger, Ch. et al. 1979b. Phys. Lett. 86B:418
Berger, Ch. et al. 1980a. DESY Report 80/117
Berger, Ch. et al. 1980b. Phys. Lett. B78:176
Berger, Ch. et al. 1980c. Phys. Lett. 97B:459
Berger, Ch. et al. 1980d. DESY Report 80/78
Berger, Ch. et al. 1980e. Phys. Lett. 90B:312
Berger, Ch. et al. 1980f. DESY Report 80/111
Berger, Ch. et al. 1981. DESY Report 81-001
Bienlein, J. K. et al. 1978. Phys. Lett. 78:360; DESY Report 80/66
Bjorken, J. D. 1969. Phys. Rev. 179:1547. See also Bjorken, J. D. and Paschos, E. A. 1969. Phys. Rev. 185:1975
Bjorken, J. D., Brodsky, S. J. 1970. Phys. Rev. D1:1416
Bjorken, J. D. 1978. Phys. Rev. D17:171
Bock, P. et al. 1980. Z. Physik C 6:125
Bodek, A. et al. 1979. Phys. Rev. D20:1471
Bollini, D. et al. 1980. XXth Int. Conf. on High Energy Physics, Madison, Wisconsin

Bonneau, G., Martin F. 1971. Nucl. Phys. B27:381
Bosetti, P. C. et al. (Aachen-Bonn-CERN-London-Oxford-Saclay) 1978. Nucl. Phys. B142:1
Boyarski, A. M. et al. 1975. Phys. Rev. Lett. 34:1357
Brandelik, R. et al. 1978a. Phys. Lett. 76B:361
Brandelik, R. et al. 1978b. Nucl. Phys. B148:189
Brandelik, R. et al. 1979a. Z. Physik C1:233
Brandelik, R. et al. 1979b. Phys. Lett. 86B:243
Brandelik, R. et al. 1980a. Z. Physik C4:87
Brandelik, R. et al. 1980b. DESY Report 80/108 and Phys.Lett. 99B:163
Brandelik, R. et al. 1980c. Phys. Lett. 94B:437
Brandelik, R. et al. 1980d. Phys. Lett. 97B:453
Brandelik, R. et al. 1981a. DESY Report 81-005 and Phys. Lett. in press
Brandelik, R. et al. 1981b. DESY Report
Brandt, S., Dahmen, H. D. 1979. Z. Physik C1:61
Brandt, S. et al. 1964. Phys. Lett. 12:57
Brandt, S. 1979. Proc. Int. Conf. High Energy Physics, Geneva, p.338
Brodsky, S. J. et al. 1978. Phys. Lett. 73B:203
Buras, A. J. 1980. Rev. Mod. Phys. 52:199
Buras, A. J., Gaemers, K.J.F. 1978. Nucl. Phys. B132:249
Burmester, J. et al. 1976. DESY Report 76/53
Burmester, J. et al. 1977. Phys. Lett. 66B:395
Cashmore, R. 1979. Proc. Int. Conf. on High Energy Physics, Geneva, p.330
Castorina, P., Nardulli, G., Preparata, G. 1980. Nucl. Phys. B163:333. See also Univ. of Bari, Report BA-GT 80/03
Celmaster, W., Gonsalves, R. J. 1979. Phys. Rev. Lett. 44:560
Chetyrkin, K. G., Kataev, A. L., Tkachev, F. V. 1979. Phys. Lett. 85B:277
Clark, A. R. et al. 1980. Phys. Rev. Lett. 45:682; 45:1465
Cordier, A. et al. 1979. Phys. Lett. 81B:389
Cords, D. 1980. Proc. XXth Int. Conf. on High Energy Physics, Madison, Wisc., DESY Report 80/92
Creutz, M. 1980. Phys. Rev. Lett. 45:313
Curci, G., Greco, M., Srivastava,Y. 1979. Nucl. Phys. B159:451

Darden, C. W. et al. 1978. Phys. Lett. 76B:246
Darriulat, P. 1980. Ann. Rev. Nucl. Part. Science 30:159
Daum, H. J., Meyer, H., Bürger, J. 1980. DESY Report 80/101 and Z. Physik C, in press
de Grand, T. A., Ng, Y. G., Tye, S.H.H. 1977. Phys. Rev. D16:3251
de Groot, J.G.H. et al. 1979. Phys. Lett. 82B:292; 82B:456; Z. Physik C 1:143
de Groot, J.G.H. et al. 1980. XXth Int. Conf. on High Energy Physics, Madison, Wisconsin
de Rujula, A. et al. 1978. Nucl. Phys. B138:387
Dine, M., Sapirstein, J. 1979. Phys. Rev. Lett. 43:668
Dokshitzer, Y. L., D'Yakonov, D. I., Troyan, S. I. 1978. Phys. Lett. 78B:290
Dokshitzer, Y. L., D'Yakonov, D. I., Troyan, S. I. 1980. Physics Reports 58:269
Donnachie, A., Landshoff, P. V. 1980. Phys. Lett. 95B:437
Donnachie, A., Shaw, G. 1980. Univ. of Manchester, Report MC-TH 80-33
Dorfan J. 1980. SLAC-PUB-2623 and Z. Physik C, in press
Duke, D. W., Roberts, R.G. 1980. Nucl. Phys. B166:243; Phys. Lett. 94B:417
Eidelman, S. I., Kurdadze, L. M., Vainstein, A. I. 1979. Phys. Lett. 82B:278
Ellis, J., Gaillard, M. K., Ross, G. G. 1976. Nucl. Phys. B111:253; (E.B130:516)
Ellis, J., Karliner, I. 1979. Nucl. Phys. B148:141
Ellis, J. 1979. Proc. 1979 Intern. Symp. on Lepton and Photon Interactions, FNAL, Batavia, Illinois p. 412; Proc. NEUTRINO '79, Int. Conf. on Neutrinos, Weak Interactions and Cosmology, Bergen, Norway (1979), Vol.1, p.451
Ellis, J., Sachrajda, C. T. 1979. Quarks and Leptons, Cargèse 1979. Plenum New York and London 1979, p.285-427
Ellis, R.K., Ross, D. A., Terrano, A. E. 1980. Phys. Rev. Lett. 45:1226 and CAL-Tech Rep. 68-785 and Nucl. Phys., in press
Ellis, S. D., Stirling, W. J. 1980. Univ. Washington Rep. RLO-1388-821
Fabricius, K. et al. 1980. Phys. Lett. 97B:431

Fahri, E. 1977. Phys. Rev. Lett. 39:1587
Feynman, R. P. 1972. Photon-Hadron Interactions, Benjamin, Reading, Mass. 1972
Field, R. D., Feynman, R. P. 1978. Nucl. Phys. B136:1
Fox, D. J. et al. 1974. Phys. Rev. Lett. 33:1504. See also Watanabe, Y. et al. 1975. Phys. Rev. Lett.35:898 and Chang, C. et al. 1975. Phys. Rev. Lett. 35:901
Fox, G. C., Wolfram, S. 1978. Phys. Rev. Lett. 41:1581
Fox, G. C., Wolfram, S. 1979. Nucl. Phys. B149:413
Fox, G. C., Wolfram, S. 1980. Z. Physik C4:237
Friedman, J. I., Kendall, H. W. 1972. Ann. Rev. Nuc. Sci. 22:203-254. See also Miller G. et al. 1972.
Fritzsch, H., Gell-Mann, M. 1972. Proc. XVI Int. Conf. on High Energy Physics, Chicago, Vol.2, p.135
Fritzsch, H., Gell-Mann, M., Leutwyler, H. 1973. Phys. Lett. 47B:365
Fritzsch, H., Streng, K. H. 1978. Phys. Lett. 74B:90
Georgi, H., Politzer, H. D. 1974. Phys. Rev. D9:416
Glück, M., Reya, E. 1979. Nucl. Phys. B156:456
Glück, M., Reya, E. 1980. Univ. of Dortmund Report DO-TH 80/7
Gonzales-Arroyo, A., Lõpez, C., Yndurãin, F. J. 1979. Nucl. Phys. B159:512; B153;161
Gordon, B. A. et al. 1979. Phys. Rev. D20:2645
Greenberg, O. W. 1964. Phys. Rev. Lett. 13:598
Gross, D. J., Wilczek, F. 1973. Phys. Rev. Lett. 30:1343; Phys. Rev. D8:3633; also 1974. Phys. Rev. D9:980
Halzen, F., Scott, D. M. 1980. Phys. Lett. 94B:405
Han, M., Nambu, Y. 1965. Phys. Rev. 139:1006
Hanson, G. G. et al. 1975. Phys. Rev. Lett. 35:1609
Hanson, G. G. 1978. 13th Renc. de Moriond, Vol.II, p.15
Hasenfratz, A., Hasenfratz, P. 1980. Phys. Lett. 93B:165
Hoyer, P. et al. 1979. Nucl. Phys. B161:34§
Jaffe, R. L., Ross, G. G. 1980. Phys. Lett. 93B:313
Kajantie, K., Pietarinen, E. 1980. Phys. Lett. 93B:269
Kogut, J. B., Susskind, L. 1974. Phys. Rev. D9:697; D9:3391
Kogut, J. B., Pearson, R. P., Shigemitsu, J. 1981. Phys. Lett. 98B:63

Koller, K., Walsh, T. F. 1977. Phys. Lett. 72B:227 (E.73B:504); 1978. Nucl. Phys. B140:449

Koller, K., Krasemann, H., Walsh, T. F. 1979. Z. Physik C1:71

Koller, K., Krasemann, H. 1979. Phys. Lett. 88B:119

Konishi, K., Ukawa, A., Veneziano, G. 1979. Phys. Lett. 80B:259; Nucl. Phys. B157:45

Kramer, G., Schierholz, G., Willrodt, J. 1978. Phys. Lett. 79B:249

Kramer, G., Schierholz, G. 1979. Phys. Lett. 82B:102

Kramer, G., Schierholz, G., Willrodt, J. 1980. Z. Physik C4:149

Lanius, K. 1980. DESY Report 80/36; see also Lanius K. et al. Z. Physik C, in press

La Rue, G. S., Fairbank, W. M., Phillips, J. D. 1979. Phys. Rev. Lett. 42:142; 42:1019(E)

Llewellyn Smith, Ch. 1980. Proc. XXth Int. Conf. on High Energy Physics, Madison, Wisconsin

Lo, C. Y., Sullivan, J. D. 1979. Phys. Lett. 86B:327

Marciano, W., Pagels, H. 1978. Phys. Reports 36:137

Marquardt, W., Steiner, F. 1980. Phys. Lett. 93B:480

Martin, F. 1979. Phys. Rev. D19:1382

Mestayer, M. D. 1978. A Measurement of the Proton Structure Functions Using Inelastic Electron Scattering, SLAC Rep. 214

Miller, G. et al. 1972. Phys. Rev. D5:528

Münster, G., Weisz, P. 1980. Phys. Lett. 96B:119

Nachtmann, O. 1974. Nucl. Phys. B78:455

Nambu, Y. 1966. Preludes in Theoretical Physics (Amsterdam), p.133

Newman, H. 1980. Proc. XXth Int. Conf. on High Energy Physics, Madison, Wisconsin

Niczyporuk, B. et al. 1981a. Phys. Rev. Lett. 46:92

Niczyporuk, B. et al. 1981b. DESY Report 81-008

Nowak, W. D., Schiller, H. 1975. Univ. Berlin Rep. PHE 75-2

Para, A., Sachrajda, C. T. 1979. Phys. Lett. 86B:331

Parisi, G., Petronzio, R. 1979. Nucl. Phys. B154:427

Pennington, M. R., Ross, G. G. 1979. Phys. Lett. 86B:371

Pennington, M. R., Ross, G. G. 1981. Nucl. Phys. B179:324

Perez-Y-Jorba, 1978. Proc. XIX Int. Conf. on High Energy Physics, Tokyo, p.277

Perkins, D. H. 1980. Acta Physica Polonica B11:39-71

Petersen, A. 1980. 15th Renc. de Moriond and DESY Report 80/46

Politzer, H. D. 1973. Phys. Rev. Lett. 30:1346

Polyakov, A. M. 1975. Proc. 7th Int. Symp. Lepton and Photon Interactions at High Energies, Stanford, p.855
Preparata, G., Valenti, G. 1981. Submitted to Phys. Rev. Lett.
Quenzer, A. 1977. Thesis, Orsay Report LAL 1294
Quirk, T. W., MacAllister, J. B., Williams, W.S.C., Tao, C. 1980. Phys. Lett. 91B:285
Rakow, P.E.L., Webber, B. R. 1979. Phys. Rev. Lett. 43:1695
Renton, P., Williams, W.S.C. 1981. Ann. Rev. Nuc. Sci., this volume
Reya, E. 1979. Phys. Lett. 84B:445
Reya, E. 1981. Phys. Reports, to be published
Riordan, E. M. et al. 1974. Phys. Lett. 52B:249; see also SLAC-PUB-1634
Schmidt-Parzefall, H. 1980. Proc. XXth Int. Conf. on High Energy Physics, Madison, Wisconsin
Schwitters, R. F. et al. 1975. Phys. Rev. Lett. 35:1320
Schwitters, R. F. 1976. XVIII Int. Conf. on High Energy Physics, Tbilisi, p.B34
Schwinger, J. 1973. Particles, Sources and Fields, Vol.II. (Addison-Wesley, New York)
Sciulli, F. 1980. Proc. XXth Int. Conf. on High Energy Physics, Madison, Wisconsin
Sidorov, V. A. 1976. Proc. XVIII Int. Conf. on High Energy Physics, Tbilisi, P. N46
Söding, P. 1979. Proc. Int. Conf. on High Energy Physics, Geneva, p.271
Sterman, E., Weinberg, S. 1977. Phys. Rev. Lett. 39:1436
't Hooft, G. 1972. Unpublished
Taylor, R. R. 1969. Proc. 4th Intern. Symp. on Electron and Photon Interactions at High Energies, Liverpool 1969. p.251
Timm, U. 1980. DESY Report 80/70
Vermaseren, J.A.M., Gaemers, K.J.F., Oldham, S.J. 1980. CERN Rep. TH 3002
Walsh, T. F., Zerwas, P. M. 1980. Phys. Lett. 93B:53
Weinberg, S. 1973. Phys. Rev. Lett. 31:494
Wiik, B. H., Wolf, G. 1979. Electron-Positron Interactions, Springer Tracts in Modern Physics, Vol. 86
Wu, S. L., Zobernig, G. 1979. Z. Physik C2:107
Yamada, S. 1980. Proc. XX Int. Conf. on High Energy Physics, Madison, Wisconsin; Univ. Tokyo Rep.